



HAL
open science

Multi-scale Geometric Modeling of Ambiguous Shapes with Toleranced Balls and Compoundly Weighted alpha-shapes

Frédéric Cazals, Tom Dreyfus

► **To cite this version:**

Frédéric Cazals, Tom Dreyfus. Multi-scale Geometric Modeling of Ambiguous Shapes with Toleranced Balls and Compoundly Weighted alpha-shapes. [Research Report] RR-7306, INRIA. 2010, pp.32. inria-00497688

HAL Id: inria-00497688

<https://inria.hal.science/inria-00497688>

Submitted on 7 Jul 2010

HAL is a multi-disciplinary open access archive for the deposit and dissemination of scientific research documents, whether they are published or not. The documents may come from teaching and research institutions in France or abroad, or from public or private research centers.

L'archive ouverte pluridisciplinaire **HAL**, est destinée au dépôt et à la diffusion de documents scientifiques de niveau recherche, publiés ou non, émanant des établissements d'enseignement et de recherche français ou étrangers, des laboratoires publics ou privés.



INSTITUT NATIONAL DE RECHERCHE EN INFORMATIQUE ET EN AUTOMATIQUE

*Multi-scale Geometric Modeling of Ambiguous
Shapes with Toleranced Balls and Compoundly
Weighted α -shapes*

Frédéric Cazals — Tom Dreyfus

N° 7306

May 2010

Thème BIO

 *R*
*apport
de recherche*

Multi-scale Geometric Modeling of Ambiguous Shapes with Toleranced Balls and Compoundly Weighted α -shapes

Frédéric Cazals^{*}, Tom Dreyfus[†]

Thème BIO — Systèmes biologiques
Projet ABS

Rapport de recherche n° 7306 — May 2010 — 29 pages

Abstract: Dealing with ambiguous data is a challenge in Science in general and geometry processing in particular. One route of choice to extract information from such data consists of replacing the ambiguous input by a continuum, typically a one-parameter family, so as to mine stable geometric and topological features within this family. This work follows this spirit and introduces a novel framework to handle 3D ambiguous geometric data which are naturally modeled by balls.

First, we introduce *toleranced balls* to model ambiguous geometric objects. A toleranced ball consists of two concentric balls, and interpolating between their radii provides a way to explore a range of possible geometries. We propose to model an ambiguous shape by a collection of toleranced balls, and show that the aforementioned radius interpolation is tantamount to the growth process associated with an additively-multiplicatively weighted Voronoi diagram (also called compoundly weighted or CW). Second and third, we investigate properties of the CW diagram and the associated CW α -complex, which provides a filtration called the λ -complex. Fourth, we propose a naive algorithm to compute the CW VD. Finally, we use the λ -complex to assess the quality of models of large protein assemblies, as these models inherently feature ambiguities.

Key-words: Union of balls, Voronoi diagrams, α -shapes, stability, topological persistence, proteins, macromolecular complexes, interfaces, structural biology.

^{*} INRIA Sophia-Antipolis-Méditerranée, Algorithms-Biology-Structure; Frederic.Cazals@sophia.inria.fr

[†] INRIA Sophia-Antipolis-Méditerranée, Algorithms-Biology-Structure; Sebastien.Loriot@sophia.inria.fr

Modélisation Multi-échelle de Formes Ambiguës avec des Boules Tolérancées et les α -shapes à Pondération Composée

Résumé : La manipulation de données ambiguës est un challenge tout à fait général, qui est particulièrement exacerbé en géométrie. Une façon intéressante d'extraire de l'information de telles données consiste à remplacer celles-ci par un continuum, typiquement une famille à un paramètre, de façon à chercher des structures géométriques et topologiques stables au sein de cette famille. Ce travail s'inscrit dans cette veine, et propose un nouveau canevas pour manipuler des données 3D ambiguës.

Tout d'abord, nous introduisons les boules tolérancées. Une telle boule est constituée de deux boules concentriques, et interpoler entre leurs rayons permet d'explorer un ensemble de géométries possibles. Nous proposons de modéliser une forme ambiguë par un ensemble de boules tolérancées, et montrons que le processus d'interpolation évoqué ci-dessus conduit à un diagramme de Voronoi additif-multiplicatif (aussi appelé à pondération composée, ou CW). Ensuite, nous nous intéressons aux propriétés du diagramme CW et à l' α -shape associée, qui représente une filtration que nous nommons le λ -complexe. Nous poursuivons par un algorithme naïf de calcul du diagramme de Voronoi CW. Enfin, nous montrons comment utiliser le λ -complexe pour étudier la qualité de modèles de gros assemblages macro-moléculaires, ces modèles présentant de façon intrinsèque des ambiguïtés.

Mots-clés : Union de boules, diagrammes de Voronoi, α -shapes, stabilité, persistance topologique, protéines, complexes macro-moléculaires, interfaces, biologie structurale.

1 Introduction

1.1 Voronoi Diagrams and Applications

The Voronoi diagram of a finite collection of sites equipped with a generalized distance is the cell decomposition of the ambient space into equivalence classes of points having the same nearest sites for this distance. Voronoi diagrams are central constructions in science and engineering [OC00], and their versatility actually comes from two sources. First, the great variability of sites and distances is a first source of diversity. While the most classical construction is the Euclidean distance diagram for points, the mere class of circles and weighted points yields as diverse diagrams as power, Apollonius and Möbius diagrams—see [BWY06] and Fig. 1. Second, the information encoded in a Voronoi diagram actually goes beyond the aforementioned cell decomposition. One can indeed consider the bisectors bounding the cells as the realization of a growth process defined by the distance, in the sense that the level sets of this distance intersect on the bisectors. This viewpoint motivated the development of α -complexes and α -shapes [Ede92], a beautiful construction providing a filtration of the Delaunay triangulation dual of the Voronoi diagram, later complemented by the flow complex [GJ03]. From a mathematical standpoint, these developments are concerned with the topological changes undergone by the sub-level sets of the distance, which is the heart of Morse theory [Mil63]. Ideas in this realm also motivated the development of topological persistence [ELZ02, CSEH05], a subject concerned with the assessment of the stability of topological features associated with the sub-level sets of a function defined on a topological space.

The success of α -shapes relies on two cornerstones. First, the aforementioned growth process gives access to a multi-scale analysis of the input sites. For example, the problem of reconstructing a shape from sample points can be tackled by considering the *space-filling diagram* consisting of balls grown around the sample points. Alas, a provably good reconstruction using this strategy requires a uniform sampling, which motivated the definition of more local growth processes. One may cite conformal α -shapes [CGPZ06], where the growth process depends on the distance of the samples to the medial axis, and the scale-axis transform [GMPW09] which provides a hierarchy of skeletal shapes based on a dilation (and retraction) of medial balls. Second, α -shapes inherently model objects represented by collections of balls—in particular molecules, and encode remarkable geometric and topological properties [Ede95]. For the particular case of proteins and small macro-molecular complexes, they have been instrumental to compute molecular surfaces [AE96] and model interfaces [BGNC09, LC10].

Our developments are precisely motivated by the requirement to perform multi-scale analysis in computational structural biology.

1.2 Contributions

Structural proteomics studies are concerned by the identification and the modeling of molecular machines operating within the cell [GAG⁺06], and a major endeavour consists of modeling assemblies involving from tens [LTSW09] to hundreds [ADV⁺07] of polypeptide chains. This modeling requires integrating data coming from several experimental sources, these data being typically noisy and incomplete [AFK⁺08]. In this context, the premises just discussed on α -shapes certainly hold: on the one hand, balls are the primitive of choice since we deal with atoms and molecules; on the other hand, multi-scale analysis are in order since we deal with ambiguous data and need to accommodate uncertainties on the shapes and positions of proteins within an assembly. In this context, we make the following contributions.

First, we introduce toleranced balls to model ambiguous geometric shapes. A toleranced ball consists of two concentric balls—the *inner* and *outer* balls, and interpolating between them allows one to replace an arbitrary ball by one-parameter family of balls. As illustrated on Fig. 2, the inner (outer) ball of a toleranced ball is meant to accommodate high (low) confidence regions. We note in passing that our approach bears some similarities with modeling with toleranced parts in engineering, where tolerances are generally accommodated thanks to Minkowski sums [LWC97]. Second, we show that the growth process associated with this interpolation is associated with a so-called additively-multiplicatively-weighted Voronoi diagram, also called compoundly weighted Voronoi diagram—CW VD for short. Third, we investigate properties of this CW diagram and its dual. Fourth, we present the filtration, called the λ -complex, induced on the dual by the growth process, and encoding all possible topologies associated with this growth process. For any value of λ , the λ -complex identifies a list of simplices of the dual complex, together with a label for each of them. This label precisely encodes the contribution of the simplex to the boundary of the union of the balls grown thanks to the additively-multiplicatively model. Our analysis generalizes the so-called β -shapes [SCC⁺06], i.e. the α -shape associated to an Apollonius diagram [BD05, BWY06, EK06]. Fifth, we present an algorithm to compute the CW VD. Finally, we present experimental results on toleranced protein models.

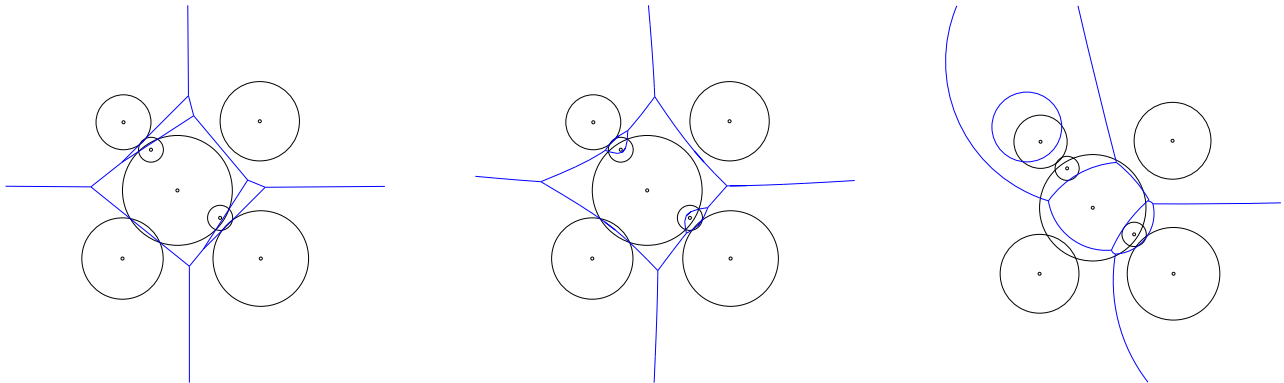


Figure 1: Curved Voronoi diagrams of 7 circles / weighted points. (Left) Power diagram $d(S_i(c_i, r_i), p) = \|p - c_i\|^2 - r_i^2$. (Middle) Apollonius diagram : $d(S_i(c_i, r_i), p) = \|p - c_i\| - r_i$ (Right) Möbius diagram : $d(S_i(c_i, a_i, r_i), p) = a_i \|p - c_i\|^2 - r_i^2$.

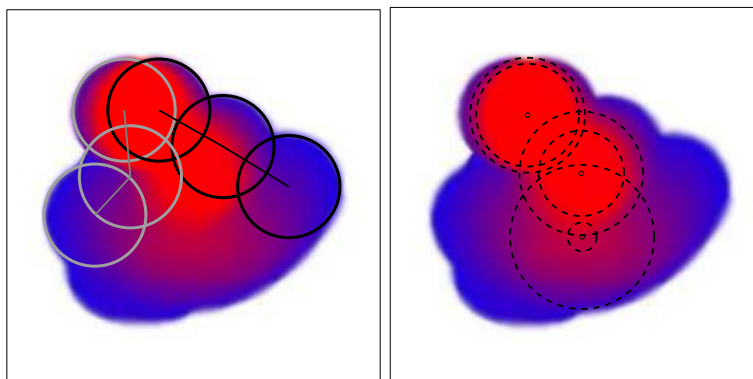


Figure 2: A fictitious molecule of three atoms undergoing conformational changes. (a) The two extreme conformations, together with the probability density map D in background. The map D displays the probability for a given point to be covered by a random conformation. (b) Three tolerated balls used to cover the portion of the map D involving probabilities beyond a given threshold. Dashed lines represent the inner and outer balls of the tolerated balls. Note that higher the confidence / probability, the smaller the region between the inner and outer balls.

2 Toleranced Models and Compoundly Weighted Voronoi Diagram

2.1 Compoundly Weighted Distance and Toleranced Balls

Toleranced balls. Given a weighted point $S_i(c_i; \mu_i, \alpha_i)$, with center c_i and parameters (real numbers) $\mu_i > 0$ and α_i , we define the additively-multiplicatively distance as follows:

$$\lambda(S_i, p) = \mu_i \|c_i p\| - \alpha_i. \quad (1)$$

This distance is associated with so-called compoundly-weighted Voronoi diagrams or CW VD for short [OC00]. Geometrically speaking, this distance is best understood using the following growth process. Let a *toleranced ball* $\overline{S}_i(c_i; r_i^-, r_i^+)$ be a pair of concentric balls of radii $r_i^- < r_i^+$, centered at c_i . These balls are called the *inner* and *outer* balls. Given a toleranced ball \overline{S}_i and a real parameter λ , consider the *grown ball* $\overline{S}_i[\lambda]$ centered at c_i and whose radius is defined by:

$$r_i(\lambda) = r_i^- + \lambda(r_i^+ - r_i^-). \quad (2)$$

Denoting $\delta_i = r_i^+ - r_i^-$, a point p is reached by this growth process once $r_i(\lambda) = \|c_i p\|$, that is

$$\lambda(\overline{S}_i, p) = \frac{\|c_i p\|}{\delta_i} - \frac{r_i^-}{\delta_i}. \quad (3)$$

In other words, a toleranced ball $\overline{S}_i(c_i; r_i^-, r_i^+)$ is tantamount to a weighted point $S_i(c_i; \mu_i = 1/\delta_i, \alpha_i = r_i^-/\delta_i)$; and reciprocally, a weighted point $S_i(c_i; \mu_i, \alpha_i)$ is tantamount to a toleranced ball $\overline{S}_i(c_i; r_i^- = \alpha_i/\mu_i, r_i^+ = (1 + \alpha_i)/\mu_i)$. In the sequel, we shall use both terminologies and exchangeably refer to weighted point S_i or toleranced ball \overline{S}_i .

2.2 On Concomitant Interpolation Processes

Consider two toleranced balls \overline{S}_i and \overline{S}_j . We term the linear interpolation of Eq. (2) *concomitant* since at $\lambda = 0$ (resp. $\lambda = 1$) the grown balls $\overline{S}_i[\lambda]$ and $\overline{S}_j[\lambda]$ respectively match their inner (outer) balls. In the context of toleranced models, concomitance is important since, for a collection of toleranced balls, we aim at exploring the region sandwiched between the inner and outer balls coherently. Interestingly, concomitance requires multiplicatively weighted Voronoi diagram — CW or Möbius.

Non concomitant interpolations. For the power diagram, the growth process consists of modifying the squared radius as follows:

$$r_i^2(\alpha) = \|c_i p\|^2 = r_i^2 + \alpha. \quad (4)$$

Let a toleranced weighted point be a pair of concentric balls of weights $r_i^2 = (r_i^-)^2$ and $(r_i^+)^2$. The value α_i required to interpolate from the inner to the outer ball is $\alpha_i = (r_i^+)^2 - (r_i^-)^2$. The interpolation is not concomitant since for two toleranced weighted points, one generically has $\alpha_i \neq \alpha_j$.

The same observation holds for the growth process associated with an Apollonius diagram, which is not concomitant unless the discrepancy $r_i^+ - r_i^-$ of all toleranced balls is equal to some constant.

Concomitant interpolations. To see that Möbius diagrams share the concomitance property with CW diagrams, recall that the generalized Möbius distance to a weighted point $S_i(c_i, \mu_i, \alpha_i)$ is defined by:

$$d(S_i, p) = \mu_i \|c_i p\|^2 + \alpha_i. \quad (5)$$

Equivalently,

$$\|c_i p\|^2 = \frac{1}{\mu_i}(d + \alpha_i). \quad (6)$$

To make the connexion between the distance of Eq. (5) and a toleranced ball, we use $d = 0$ and $d = 1$, which yields

$$(r_i^-)^2 = \frac{\alpha_i}{\mu_i}, \text{ and } (r_i^+)^2 = \frac{1 + \alpha_i}{\mu_i}. \quad (7)$$

Equivalently, one has:

$$\mu_i = \frac{1}{(r_i^+)^2 - (r_i^-)^2} \text{ and } \alpha_i = \frac{(r_i^-)^2}{(r_i^+)^2 - (r_i^-)^2}. \quad (8)$$

A comparison of the CW and Möbius growth models, that is $r_i(\lambda) = \|c_i p\|$ versus $r_i(d) = \sqrt{\|c_i p\|^2}$, is provided on Fig. 3. Compared to the CW linear growth model and as shown by the variation of the derivative of $\partial r_i(d)/\partial d$, a large difference $(r_i^+)^2 - (r_i^-)^2$ biases the Möbius interpolation towards small values.

2.3 Toleranced Tangency and Generalization of the Empty Ball Property

For affine (Apollonius) Voronoi diagrams, it is well known that for each point centered on a Voronoi face, there exists a unique ball orthogonal (tangent) to the balls associated with the vertices of the dual simplex, and conflict free with all the other balls¹. To derive the analogue in the CW-case, consider a point p and two toleranced balls \overline{S}_i and \overline{S}_j such that $\lambda(S_i, p) = \lambda < \lambda(S_j, p)$. For the pair \overline{S}_i and p , one gets with Eq. (1):

$$\|p c_i\| - \frac{\alpha_i}{\mu_i} - \frac{\lambda}{\mu_i} = 0 \Leftrightarrow \|p c_i\| - r_i^- - \lambda \delta_i = 0. \quad (9)$$

¹Consider e.g. the power case, and pick a point p on the Voronoi face dual of a simplex involving a ball $S_i(c_i, w_i)$. Assume that point p lies on the sphere bounding the ball $S_i(c_i, w_i + \alpha)$. One has $\pi(p, S_i) = \|c_i p\|^2 - w_i - \alpha = 0$, or equivalently, the balls S_i and $X(p, \alpha)$ are orthogonal.

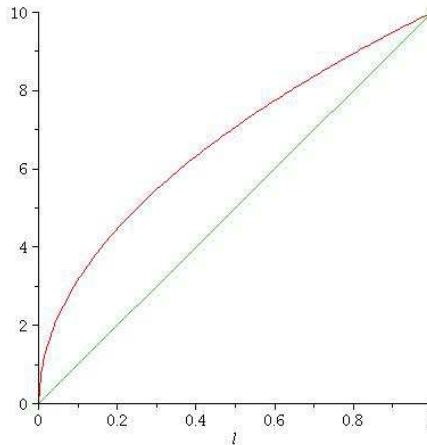


Figure 3: Comparing the variation of the radius for the CW model (green curve) and the Möbius model (red curve). On this example, $r_i^- = 0$ and $r_i^+ = 10$.

Similarly, for the pair \overline{S}_j and point p :

$$\|pc_j\| - \frac{\alpha_j}{\mu_j} - \frac{\lambda}{\mu_j} > 0 \Leftrightarrow \|pc_j\| - r_j^- - \lambda\delta_j > 0. \quad (10)$$

We summarize with the following definition, illustrated on Fig.4:

Definition. 1. A ball $B(p, \lambda)$ which satisfies the condition of Eq. (9) w.r.t. a toleranced ball \overline{S}_i is called toleranced tangent (TT for short) to \overline{S}_i . A toleranced ball \overline{S}_j and a ball $B(p, \lambda)$ which satisfy the condition of Eq. (10) are called conflict free.

Remark. 1. Equation (9) states that the inner ball $B(c_i, r_i^-)$ and the ball $B(p, \lambda\delta_i)$ —which is the ball $B(p, \lambda)$ scaled by δ_i , are tangent. Similarly, condition (10) states that $B(c_j, r_j^-)$ and $B(p, \lambda\delta_j)$ do not intersect. We shall use this property to illustrate TT balls, see e.g. Fig. 4.

Remark. 2. Let $\overline{\mathcal{S}}$ be a collection of toleranced balls. Consider a ball $B(p, \lambda)$ which is TT to a subset of balls $T \subset \overline{\mathcal{S}}$, and conflict free with the toleranced balls in $\overline{\mathcal{S}} \setminus T$. The center p of this ball is found at the intersection of the spheres bounding the grown balls $\overline{S}_i[\lambda]$ with $\overline{S}_i \in T$, and is located outside the grown balls $\overline{S}_j[\lambda]$ with $\overline{S}_j \in \overline{\mathcal{S}} \setminus T$.

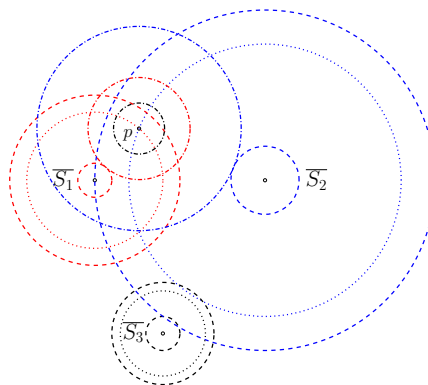


Figure 4: Toleranced tangent (TT) balls and conflict free balls. In dashed lines, toleranced balls $\overline{S}_1(0, 0; 1, 5)$, $\overline{S}_2(0, 10; 2, 8)$, $\overline{S}_3(4, -9; 1, 3)$. The three dotted circles represent $\overline{S}_1[3/4]$, $\overline{S}_2[3/4]$, $\overline{S}_3[3/4]$. The three circles centered at p are the scaled versions of ball $B(p, 3/4)$; following remark 1, ball $B(p, 3/4)$ is TT to \overline{S}_1 and \overline{S}_2 , and conflict free with \overline{S}_3 .

Remark. 3. In Eq. (9) and (10), the radius of the toleranced ball $B(p, \lambda\delta_i)$ depends on the parameter δ_i from toleranced ball \overline{S}_i . Denoting δ^+ the additively weighted distance between two weighted points, Eq. (9) and Eq.

(10) may be rewritten as follow:

$$\delta^+(B(p, \lambda), B(p_i, \frac{r_i^-}{\delta_i})) = \frac{\delta_i - 1}{\delta_i} \|pp_i\|, \quad (11)$$

and

$$\delta^+(B(p, \lambda), B(p_i, \frac{r_i^-}{\delta_i})) > \frac{\delta_i - 1}{\delta_i} \|pp_i\|. \quad (12)$$

The left-hand side involves $B(p, \lambda)$, a ball whose radius does not depend on parameters from toleranced balls of $\overline{\mathcal{S}}$, as for the power and Apollonius cases. But the right-hand-side is parametrized. In the sequel, we use Eq. (9) and Eq. (10) for a simpler geometric interpretation of toleranced tangency and conflict-ness. A generic ball not belonging to $\overline{\mathcal{S}}$ will be denoted $B(p, \lambda)$.

3 The Compoundly Weighted Voronoi Diagram

Consider a collection $\overline{\mathcal{S}}$ of n toleranced balls. The Compoundly Weighted Voronoi diagram is the partition of the space according to the *nearest neighbor* relationship, for the CW distance, that is:

$$Vor(\overline{\mathcal{S}}_i) = \{p \in \mathbb{R}^3 \mid \lambda(\overline{\mathcal{S}}_i, p) \leq \lambda(\overline{\mathcal{S}}_j, p) \forall j \neq i\}. \quad (13)$$

More generally, denoting T_{k+1} a tuple of $k+1$ toleranced balls, we are interested in $Vor(T_{k+1}) = \cap_{\overline{\mathcal{S}}_i \in T_{k+1}} Vor(\overline{\mathcal{S}}_i)$. Naturally, we are also interested in the dual complex generalizing the Delaunay triangulation.

3.1 Bisectors in the CW Case

The bisector of a tuple of toleranced balls T_{k+1} is the loci of points having the same CW distance w.r.t. every toleranced ball. We denote this bisector $\zeta(T_{k+1})$, and examine in turn the case for pairs, triples, and quadruples. Our analysis assumes that the δ_i are not equal, as this is the Apollonius case [BWY06].

3.1.1 Bisector of two toleranced balls

Analysis. Let $\overline{\mathcal{S}}_i$ and $\overline{\mathcal{S}}_j$ be two toleranced balls. The following property describes the existence of the bisector $\zeta(i, j)$ of $\overline{\mathcal{S}}_i$ and $\overline{\mathcal{S}}_j$:

Proposition. 1. $\overline{\mathcal{S}}_i$ is trivial w.r.t. toleranced ball $\overline{\mathcal{S}}_j$ iff $\delta_i \leq \delta_j$ and the following condition, which states that c_i belongs to the interior of the Voronoi region of $\overline{\mathcal{S}}_j$, holds:

$$\lambda(\overline{\mathcal{S}}_j, c_i) < -\frac{r_i^-}{\delta_i}. \quad (14)$$

Proof. If the Voronoi region V_i of $\overline{\mathcal{S}}_i$ is empty, one has in particular, $c_i \notin V_i$, which is exactly Eq. (14). The second implication also trivial holds. For the converse, applying the definition of $\lambda(\overline{\mathcal{S}}_i, p)$ to any point p , we get:

$$\lambda(\overline{\mathcal{S}}_i, p) = \frac{\|pc_i\| - r_i^-}{\delta_i} > \frac{\|pc_i\|}{\delta_i} + \frac{\|c_i c_j\| - r_j^-}{\delta_j} \quad (15)$$

$$\geq \frac{\|pc_i\| + \|c_i c_j\| - r_j^-}{\delta_j} \quad (16)$$

$$> \frac{\|pc_j\| - r_j^-}{\delta_j} = \lambda(\overline{\mathcal{S}}_j, p). \quad (17)$$

The three derivations respectively stem from Eq. (14), from $\delta_i \leq \delta_j$, and from the triangle inequality. \square

Assuming that $\zeta(i, j)$ exists, its geometry depends on the relative values of δ_i and δ_j . Assuming w.l.o.g. that $\delta_i < \delta_j$, $\overline{\mathcal{S}}_j$ grows faster than $\overline{\mathcal{S}}_i$ so that for a large enough value of λ , the grown ball $\overline{\mathcal{S}}_i[\lambda]$ is contained in its counterpart $\overline{\mathcal{S}}_j[\lambda]$, so that the bisector is a closed surface, with c_i in the bounded region delimited by $\zeta(i, j)$. Matching the generalized distances shows that this surface is a degree-four algebraic surface. See Fig. 5 for a 2D illustration.

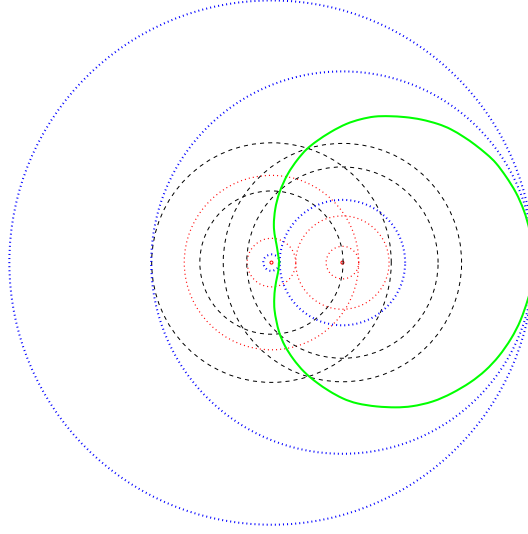


Figure 5: Two tolerated balls and their bisector which is a degree four algebraic curve –green curve. Dashed circles corresponding to the inner and outer balls. Dotted circles correspond to the solutions of a degree four equation : blue ones are tolerated tangent circles, red ones are algebraic artifacts.

Extremal TT balls. If the bisector exists, it makes sense to track the TT balls such that the corresponding λ value is a local extremum. By radial symmetry w.r.t. the line joining the centers of the balls, such balls are necessarily centered at the intersection between the bisector and the line joining the centers. Assume w.l.o.g. that $\delta_i < \delta_j$. The minimal such ball, denoted $\underline{M}_{i,j}(\underline{m}_{i,j}, \underline{\rho}_{i,j})$ is such that $\overline{S}_i[\underline{\rho}_{i,j}]$ and $\overline{S}_j[\underline{\rho}_{i,j}]$ are tangent at $\underline{m}_{i,j}$. The maximal ball $\overline{M}_{i,j}(\overline{m}_{i,j}, \overline{\rho}_{i,j})$ is such that $\overline{S}_i[\overline{\rho}_{i,j}]$ is interior-tangent to $\overline{S}_j[\overline{\rho}_{i,j}]$ at $\overline{m}_{i,j}$.

Remark. 4. As illustrated on Fig. 6, $\overline{S}_j[\underline{\rho}_{i,j}]$ may be exterior or interior to $\overline{S}_i[\underline{\rho}_{i,j}]$; Ball $\overline{S}_j[\underline{\rho}_{i,j}]$ is interior to $\overline{S}_i[\underline{\rho}_{i,j}]$ iff \overline{S}_i is closer to c_j than \overline{S}_j for the CW distance i.e. $\lambda(\overline{S}_i, c_j) < \lambda(\overline{S}_j, c_j)$. In the limit case $\lambda(\overline{S}_i, c_j) = \lambda(\overline{S}_j, c_j)$, $c_j = \underline{m}_{i,j}$ and $\overline{S}_j[\underline{\rho}_{i,j}]$ may be considered as exterior to $\overline{S}_i[\underline{\rho}_{i,j}]$.

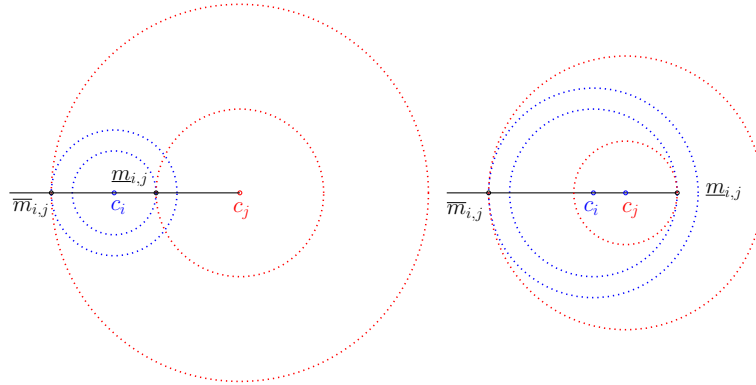


Figure 6: Relative position of minimal and maximal TT balls of two balls (Left) $\overline{S}_j[\underline{\rho}_{i,j}]$ and $\overline{S}_i[\underline{\rho}_{i,j}]$ are exterior tangent (Right) $\overline{S}_j[\underline{\rho}_{i,j}]$ is interior tangent to $\overline{S}_i[\underline{\rho}_{i,j}]$.

The parameters of these extremal TT balls are computed as follows:

Proposition. 2. The two extremal TT balls $B(p, \lambda)$ of two tolerated balls are characterized by

$$\lambda = \frac{\|c_i c_j\| - (\alpha r_i^- + \beta r_j^-)}{\alpha \delta_i + \beta \delta_j}, \quad (18)$$

and

$$c_i \vec{p} = \alpha \frac{\lambda \delta_i + r_i^-}{\|c_i c_j\|} c_i \vec{c}_j, \quad (19)$$

where $\alpha = \pm 1$ and $\beta = \pm 1$ depend on the ball processed (minimal or maximal) and the relative positions of \overline{S}_i and \overline{S}_j (case analysis in the proof).

Proof. Denote $\vec{u}_{p,p'}$ the unit vector between two points p and p' . The extremal TT ball $\overline{M}_{i,j} = (p, \lambda)$ or $\overline{M}_{i,j} = (p, \lambda)$ of \overline{S}_i and \overline{S}_j being centered on the line joining the centers c_i and c_j , we can express the weight λ as follows:

$$c_i \vec{p} + p \vec{c}_j = c_i \vec{c}_j \quad (20)$$

$$\Leftrightarrow \|c_i p\| \vec{u}_{c_i p} + \|p c_j\| \vec{u}_{p c_j} = \|c_i c_j\| \vec{u}_{c_i c_j} \quad (21)$$

$$\Leftrightarrow \|c_i p\| \vec{u}_{c_i p} \cdot \vec{u}_{c_i c_j} + \|p c_j\| \vec{u}_{p c_j} \cdot \vec{u}_{c_i c_j} = \|c_i c_j\| \quad (22)$$

$$\alpha(\lambda \delta_i + r_i^-) + \beta(\lambda \delta_j + r_j^-) = \|c_i c_j\|, \quad (23)$$

where $\alpha = \vec{u}_{c_i p} \cdot \vec{u}_{c_i c_j} = \pm 1$ and $\beta = \vec{u}_{p c_j} \cdot \vec{u}_{c_i c_j} = \pm 1$. Equation (18) follows easily. We note in passing that following remark 4, the signs of the dot products α and β are obtained from the sign of the expression $\lambda(\overline{S}_i, c_j) - \lambda(\overline{S}_j, c_j)$.

The weight of the extremal TT balls being determined, the center is computed as follows:

$$\alpha \vec{u}_{c_i p} = \vec{u}_{c_i c_j} \quad (24)$$

$$\Leftrightarrow \alpha \frac{c_i \vec{p}}{\|c_i p\|} = \frac{c_i \vec{c}_j}{\|c_i c_j\|} \quad (25)$$

$$\Leftrightarrow c_i \vec{p} = \alpha \frac{\|c_i p\|}{\|c_i c_j\|} c_i \vec{c}_j \quad (26)$$

$$\Leftrightarrow c_i \vec{p} = \alpha \frac{\lambda \delta_i + r_i^-}{\|c_i c_j\|} c_i \vec{c}_j. \quad (27)$$

□

3.1.2 Bisector of three toleranced balls

Analysis. Consider three toleranced balls $\overline{S}_{i_0}, \overline{S}_{i_1}, \overline{S}_{i_2}$ such that the bisector of each pair exists. To avoid the Apollonius case, we suppose without loss of generality that $\delta_{i_0} \leq \delta_{i_1} \leq \delta_{i_2}$ with $\delta_{i_0} < \delta_{i_2}$. If there is no intersection between $\zeta(i_0, i_1)$ and $\zeta(i_0, i_2)$, $\zeta(i_0, i_1, i_2)$ does not exist, and reciprocally. Assume that $\zeta(i_0, i_1, i_2)$ exists. Since at least one δ_i differs from the other two, there is at most one Apollonius bisector. The geometry of $\zeta(i_0, i_1, i_2)$ depends on $\delta_{i_0}, \delta_{i_1}$ and δ_{i_2} , and the following cases are illustrated on Fig. 7.

▷ **CWB.III.1** If there is no Apollonius bisector, $\zeta(i_0, i_1, i_2)$ is a bounded curve resulting from the intersection of two CW bisectors.

▷ **CWB.III.2** If the Apollonius bisector is not a half straight line, $\zeta(i_0, i_1, i_2)$ is a bounded curve resulting from the intersection of one CW bisector, and one sheet of a hyperboloid (possibly degenerated to a hyperplane).

▷ **CWB.III.3** If the Apollonius bisector is a half straight line, $\zeta(i_0, i_1, i_2)$ is reduced to at most two intersection points. Note that if there are two intersection points, $\delta_{i_1} = \delta_{i_2}$ and \overline{S}_{i_1} is included in and tangent to \overline{S}_{i_2} .

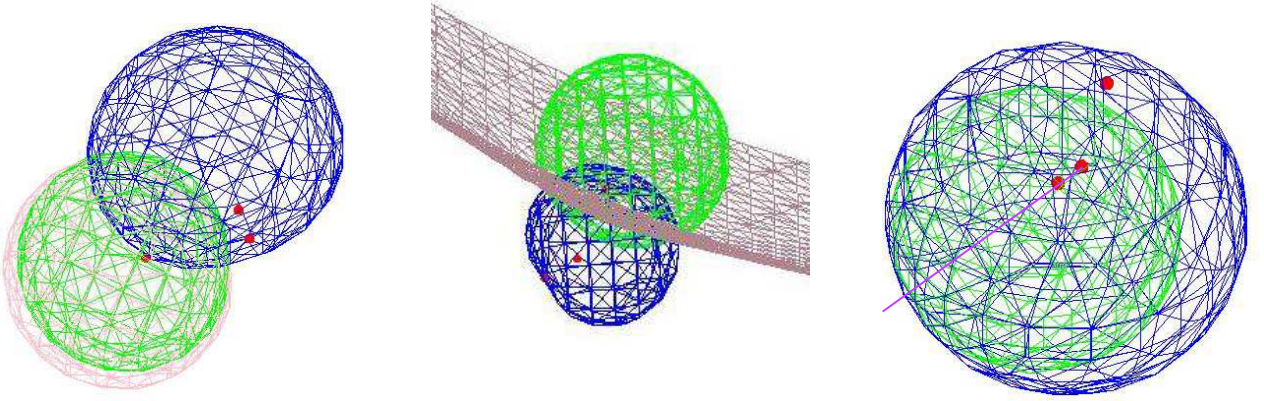


Figure 7: Bisectors of three tolerated balls. The red dots are the centers of the tolerated balls and the pink/green/blue surfaces respectively represent the bisectors $\zeta(0,1)$ / $\zeta(0,2)$ / $\zeta(1,2)$. (Left) **CWB.III.1** No Apollonius bisector (Middle) **CWB.III.2** One Apollonius bisector (Right) **CWB.III.3** One degenerate Apollonius bisector.

Extremal TT balls. In any case, there are two (possibly identical) extremal TT balls. If one bisector is a half straight line, these balls are found by intersecting this line with one of the other two bisectors.

In the general case, identifying these two balls involves four equations in four unknowns—the coordinates of the center and the weight λ . Denote π the plane defined by the centers of the three balls. The growth of the balls being symmetric with respect to this plane, the fourth equation consists of constraining the center of an extremal TT ball to plane π . The calculation is covered by the following proposition for $k = 2$:

Proposition. 3. *Let $T_{k+1} = \{\overline{S_{i_j}}\}_{j=0,\dots,k}$ be a triple or quadruple of tolerated balls, i.e. $k = 2$ or $k = 3$. Computing the two extremal TT balls of the tuple T_{k+1} requires solving a degree four equation. A value solution λ of this equation is valid provided that $\lambda\delta_{i_j} + r_{i_j}^- \geq 0$, $\forall j = 0, \dots, k$.*

Proof. of Prop. 3 for $T_{k+1} = \{\overline{S_{i_0}}, \overline{S_{i_1}}, \overline{S_{i_2}}\}$.

The ball sought has to be TT to each of the three tolerated balls, as specified by Eq. (9). Assume that the plane containing the centers of the three balls has equation $a_x x + a_y y + a_z z = a_C$. Squaring the three equations of tolerated tangency yields the system:

$$\begin{cases} (p - c_{i_0})^2 = (\lambda\delta_{i_0} + r_{i_0}^-)^2 \\ (p - c_{i_1})^2 = (\lambda\delta_{i_1} + r_{i_1}^-)^2 \\ (p - c_{i_2})^2 = (\lambda\delta_{i_2} + r_{i_2}^-)^2 \\ a_x x + a_y y + a_z z = a_C \end{cases} \quad (28)$$

Subtracting the first squared equation from the two subsequent ones yields:

$$\begin{cases} (p - c_{i_0})^2 = (\lambda\delta_{i_0} + r_{i_0}^-)^2 \\ 2p(c_{i_1} - c_{i_0}) = (\lambda\delta_{i_0} + r_{i_0}^-)^2 - (\lambda\delta_{i_1} + r_{i_1}^-)^2 - (c_{i_0}^2 - c_{i_1}^2) \\ 2p(c_{i_2} - c_{i_0}) = (\lambda\delta_{i_0} + r_{i_0}^-)^2 - (\lambda\delta_{i_2} + r_{i_2}^-)^2 - (c_{i_0}^2 - c_{i_2}^2) \\ a_x x + a_y y + a_z z = a_C \end{cases} \quad (29)$$

Using Gaussian elimination on the last three equations, one obtains three linear equations for the coordinates of p , parametrized by λ^2 . Injecting these quantities into the first equation yields the quartic equation in λ . Note that a solution is valid iff $\lambda\delta_{i_j} + r_{i_j}^- \geq 0$, and sorting the valid values yields the extreme TT balls. Also note that the coordinates of point p are rational fractions in λ^2 . □

Remark. 5. *Geometrically, three intersecting spheres generically intersect into two points. The extreme TT balls correspond to the situations where these two points coalesce.*

3.1.3 Bisector of four toleranced balls

Analysis. Consider four toleranced balls $\overline{S_{i_0}}, \overline{S_{i_1}}, \overline{S_{i_2}}, \overline{S_{i_3}}$ such that the bisector of each pair exists. To avoid the Apollonius case, we suppose w.l.o.g. that $\delta_{i_0} \leq \delta_{i_1} \leq \delta_{i_2} \leq \delta_{i_3}$ with $\delta_{i_0} < \delta_{i_3}$. If the intersection of $\zeta(i_0, i_1)$, $\zeta(i_0, i_2)$ and $\zeta(i_0, i_3)$ is empty, the intersection of all bisectors of pairs is empty and $\zeta(i_0, i_1, i_2, i_3)$ does not exist, and reciprocally. If $\zeta(i_0, i_1, i_2, i_3)$ exists, we have $\zeta(i_0, i_1, i_2, i_3) = \zeta(i_0, i_3) \cap \zeta(i_1, i_2, i_3)$, from which the following analysis follows.

▷ **CWB.IV.1** The bisectors $\zeta(i_0, i_3)$ and $\zeta(i_1, i_2, i_3)$ being a surface and a curve, their generic intersection, if any, consists of a finite set of points. As we shall see below, there are at most four such points.

▷ **CWB.IV.2** As a degenerate case, when $\zeta(i_1, i_2, i_3)$ is a bounded curve, the intersection of $\zeta(i_1, i_2, i_3)$ and $\zeta(i_0, i_3)$ may be $\zeta(i_1, i_2, i_3)$. In this case, $\zeta(i_0, i_1, i_2, i_3)$ has the geometry of the bisector $\zeta(i_1, i_2, i_3)$ of three toleranced balls.

Extremal TT balls. We distinguish two cases. If $\zeta(i_0, i_1, i_2, i_3)$ has the geometry of a bisector of three toleranced balls, we refer to the analysis carried out in section 3.1.2. Otherwise, $\zeta(i_0, i_1, i_2, i_3)$ is reduced to at most four points, as shown by the following constructive proof of proposition 3:

Proof. of Prop. 3 for $T_{k+1} = \{\overline{S_{i_0}}, \overline{S_{i_1}}, \overline{S_{i_2}}, \overline{S_{i_3}}\}$.

The ball sought has to be TT to each of the four toleranced balls, that is $\|pc_{i_j}\| = \lambda\delta_{i_j} + r_{i_j}^-$ for $j = 0, 1, 2, 3$. Squaring the four equations of toleranced tangency yields the system

$$\begin{cases} (p - c_{i_0})^2 = (\lambda\delta_{i_0} + r_{i_0}^-)^2 \\ (p - c_{i_1})^2 = (\lambda\delta_{i_1} + r_{i_1}^-)^2 \\ (p - c_{i_2})^2 = (\lambda\delta_{i_2} + r_{i_2}^-)^2 \\ (p - c_{i_3})^2 = (\lambda\delta_{i_3} + r_{i_3}^-)^2 \end{cases} \quad (30)$$

As for the case of three toleranced balls, we use Gaussian eliminations on system (30) to get three equations linear to the coordinates of p and parametrized by λ^2 , and one quartic equation on λ . Checking that $\|pc_{i_j}\| \geq 0$ provides the valid solutions, and sorting these provides the extremal solutions. \square

Remark. 6. As illustrated on Fig. 8, the system (30) may have four distinct solutions λ_i such that $\lambda_i\delta_j + r_i^- \geq 0$.

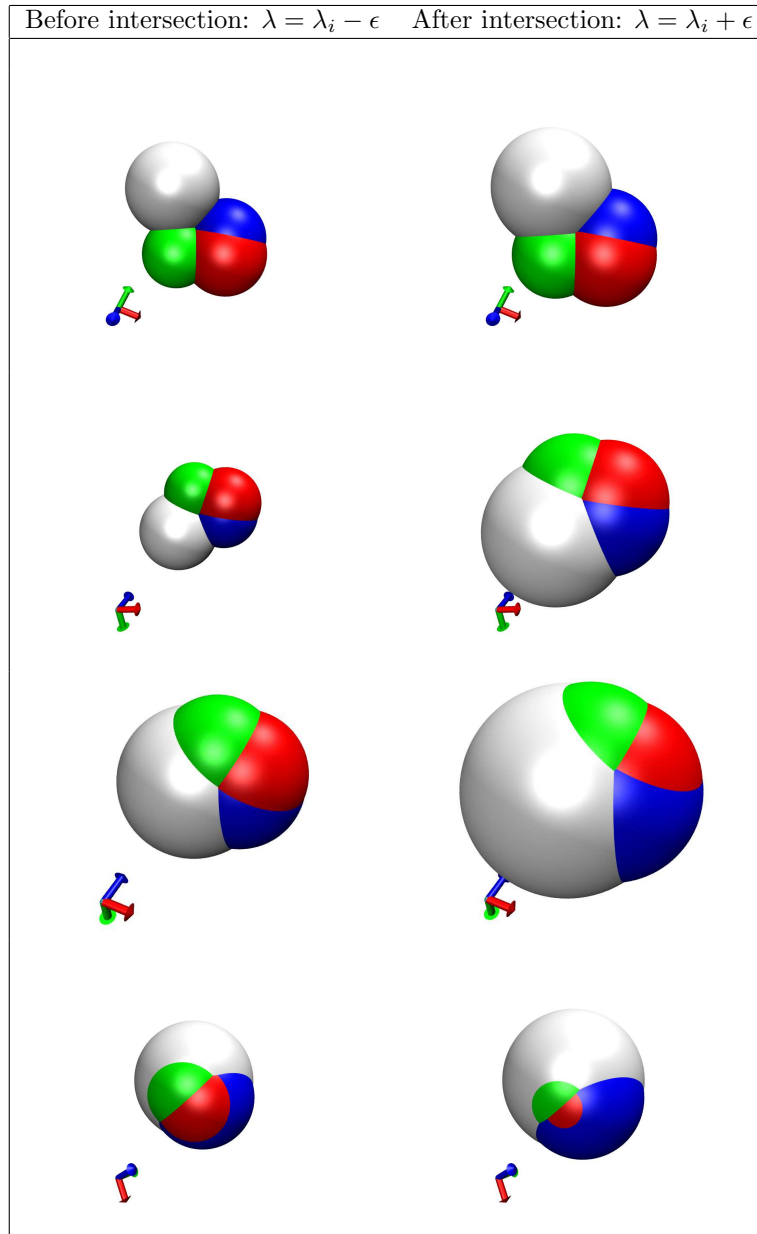


Figure 8: Upon growing, four tolerated balls may intersect into four distinct points. Denoting ϵ an arbitrarily small number, we display the tolerated balls $\overline{S}_i[\lambda_j \pm \epsilon]$. The λ_j have been sorted by increasing value from **Top** to **Bottom**.

3.2 Voronoi Diagram and its Dual Complex

Empty Voronoi regions. A tolerated ball whose region is empty is called trivial. Proposition 1 gives a condition of triviality for two tolerated balls. But triviality of a tolerated ball amidst a collection of balls is more complex since a tolerated ball might not be trivial w.r.t. any other one, yet, it might be trivial with respect to their union. To see why, observe that Eq. (13) tells us that a point in space is attributed to the Voronoi region of a tolerated ball provided that this tolerated ball *reaches* this point first in the growth process. Thus, a growing ball which is always contained in the union of a collection of growing balls is trivial, although it might not be trivial with any of them. Denoting T a collection of tolerated balls, and for any value of λ , the following condition, illustrated on Fig. 10, must hold for \overline{S}_i to be trivial:

$$\overline{S}_i[\lambda] \subset \bigcup_{\overline{S}_j \in T} \overline{S}_j[\lambda]. \quad (31)$$

Remark. 7. The triviality condition is more complex than in the Apollonius case, where a ball is hidden if and only if it is included within another ball.

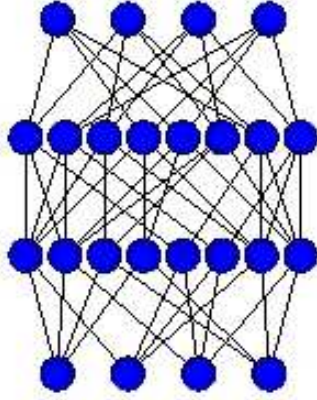


Figure 9: Dual complex of the four balls of Fig. 8—bottom and top rows respectively represent 0-simplices and 3-simplices.

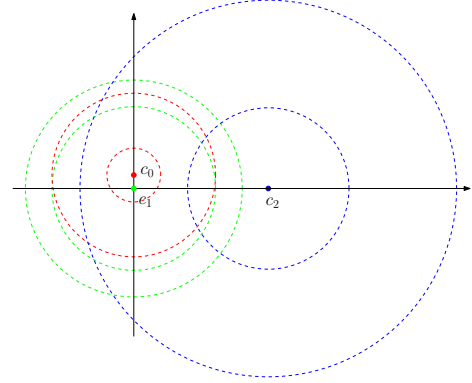


Figure 10: Hidden tolerated ball. $\overline{S}_0 = (0, 1/2; 1, 3)$ (red), $\overline{S}_1 = (0, 0; 3, 4)$ (green) and $\overline{S}_2 = (5, 0; 3, 7)$ (blue). Ball \overline{S}_0 is neither trivial w.r.t. \overline{S}_1 nor \overline{S}_2 , but is trivial with respect to both.

Dual Complex. The Voronoi region $Vor(T_{k+1})$ of a tuple T_{k+1} may have several connected components, each being termed a *face*. Each such face corresponds to the intersection of $k + 1$ Voronoi regions, so that we associate an *abstract simplex* or *simplex* for short in the dual complex. That is, if $Vor(T_{k+1})$ consists of m faces, one finds $\Delta_j(T_{k+1}), j \in 1, \dots, m$ simplices in the dual complex. (The multiplicity is omitted if the tuple T_{k+1} yields a single simplex.) The dual of a simplex $\Delta(T)$ is denoted $\Delta(T)^*$. Assuming that the input tolerated balls are numbered from 1 to n , a simplex is *identified* by a list of integers, and inclusion between such lists defines a partial order on simplices. We therefore represent the dual complex by a Hasse diagram D_S with one node per simplex. The nodes of D_S corresponding to k -simplices are denoted $D_S(k)$. Note that we may also (arbitrarily) embed a simplex within the union of Voronoi faces it is associated with. See Figs. 11, 12 and 13 for a 2D illustration.

Topological complications. A Voronoi region gets sandwiched between two neighbors when the corresponding tolerated ball defines a *lens* between the Voronoi region of two neighboring tolerated balls, a case also found in the Apollonius diagram. In the dual complex, the vertex of this tolerated balls has exactly two neighbors and the triangle corresponding to these three tolerated balls does not have any coface.

A Voronoi region might not be connected, and this may happen for tuples of size one to four. We illustrate this in 2D with Fig. 11. For a tolerated ball, consider \overline{S}_4 whose Voronoi region is split into two faces, associated with the vertices (zero-dimensional simplices) $\Delta_1(4)$ and $\Delta_2(4)$ in the Hasse diagram. For two tolerated balls, note that the Voronoi region $Vor(\overline{S}_1, \overline{S}_2)$ consists of two faces—open line segments in this case, yielding the simplices $\Delta_1(1, 2)$ and $\Delta_2(1, 2)$ in the Hasse diagram. For three tolerated balls, note that the triple $(\overline{S}_1, \overline{S}_2, \overline{S}_4)$ corresponds to two triangles.

A Voronoi region may not be simply connected. When one tolerated ball punches a hole into a face, the corresponding one-simplex does not have any coface. See e.g. tolerated ball \overline{S}_7 and the simplex $\Delta(2, 7)$ on Fig. 11. When two tolerated balls punch a hole into a Voronoi region, the two-simplex they define does not have any coface either. Finally when three tolerated balls punch a hole into a Voronoi region, two tetrahedra of the dual complex share the same vertices, the same edges and same triangles. This latter case is illustrated in 2D, where a hole punched by two tolerated balls in a Voronoi region results in two triangles with the same vertices and the same edges. See $\Delta_1(2, 5, 6)$ and $\Delta_2(2, 5, 6)$ on Fig. 11.

Bounded and Unbounded Voronoi regions. A tolerated ball $\overline{S}_i \in \overline{\mathcal{S}}$ is called *maximal* w.r.t. to $\overline{\mathcal{S}}$ if $\delta_i \geq \delta_j, \forall j \neq i$. A tolerated ball which is not maximal has a bounded Voronoi region in the CW VD of $\overline{\mathcal{S}}$, and the subset of maximal tolerated balls is denoted $\overline{\mathcal{S}}_{\max}$. The CW VD diagram of tolerated balls in $\overline{\mathcal{S}}_{\max}$ is an Apollonius diagram since all δ_i are equal, and a subset of balls in $\overline{\mathcal{S}}_{\max}$ have an unbounded Voronoi region.

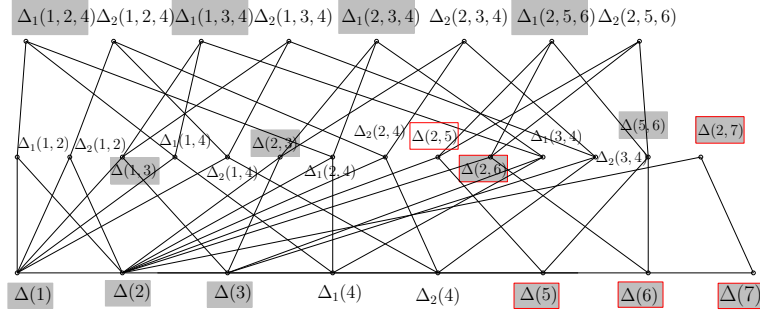


Figure 13: Hasse diagram of simplices of the dual complex of the Voronoi diagram of Fig. 11. The three lines respectively corresponding to 0-simplices, 1-simplices, and 2-simplices. Grey boxes correspond to Gabriel simplices, and boxes with a red boundary mark dominated simplices. See text for details.

Mimicking the affine case, a simplex is said to lie on the convex hull $CH(\overline{\mathcal{S}})$ of the dual complex if its dual Voronoi face is unbounded. The vertices of such simplices belong to $\overline{\mathcal{S}}_{\max}$.

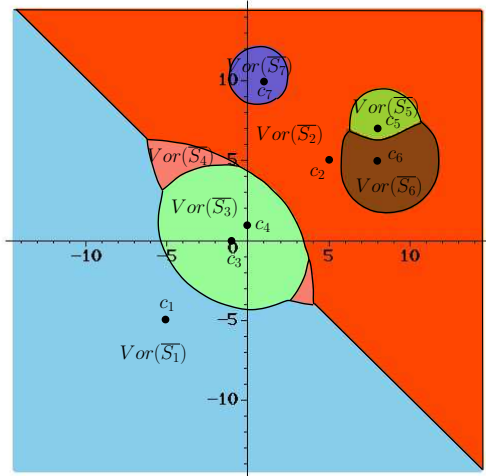


Figure 11: The CW VD of 7 tolerated balls in 2D: $\overline{S}_1 = (-5, -5; 3, 7)$, $\overline{S}_2 = (5, 5; 3, 7)$, $\overline{S}_3 = (-1, 0; 4, 5)$, $\overline{S}_4 = (0, 0; 2, 5)$, $\overline{S}_5 = (8, 7; 2, 3)$, $\overline{S}_6 = (8, 5; 3, 4)$, $\overline{S}_7 = (1, 10; 1, 2)$. $Vor(\overline{S}_3)$ and $Vor(\overline{S}_1, \overline{S}_2)$ are not connected. $Vor(\overline{S}_2)$ is not simply connected. δ_1 and δ_2 are maximal and $\overline{S}_1, \overline{S}_2$ have unbounded Voronoi regions.

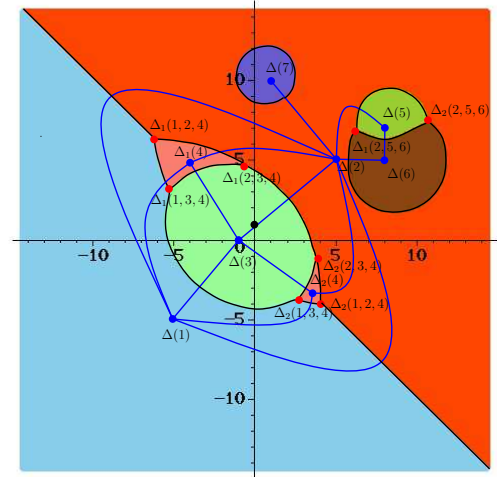


Figure 12: Dual complex for the CW VD of Fig. 11 : 0-simplices: black dots; one-simplices: blue curves; two simplices: red dots. Note that \overline{S}_4 is represented by two vertices $\Delta_1(4)$ and $\Delta_2(4)$. $\Delta_1(2, 5, 6)$ and $\Delta_2(2, 5, 6)$ share the three same edges. $\Delta(2, 7)$ does not bound any triangle.

4 Space-filling diagram and λ -complex

In this section, we investigate the domain $\mathcal{F}_\lambda = \cup \overline{S}_i[\lambda]$ defined by the union of growing balls. We present the λ -complex filtration of the dual complex. The reader is referred to [Ede92] for the affine weighted α -complex.

4.1 Gabriel, Dominant and Dominated simplices

In the affine case, changes in the α -complex are associated with Gabriel simplices: a Gabriel simplex $\Delta(T)$ is a simplex such that its minimal orthogonal ball \underline{M}_T is conflict free, and the simplex enters the α -complex when $\lambda \geq \rho_T$, with ρ_T the weight of \underline{M}_T . The generalization to the CW setting is not straightforward since

Voronoi regions might not be connected, and since a tuple T generally has two extremal TT balls, respectively denoted $\underline{M}_T(\underline{m}_T, \underline{\rho}_T)$ and $\overline{M}_T(\overline{m}_T, \overline{\rho}_T)$. We now examine these two balls and refer the reader to Fig. 14 for an illustration. (To examine this figure, recall that a TT ball $M(p, \lambda)$ is conflict free with a toleranced ball \overline{S}_i iff the scaled version of M by δ_i i.e. $M(p, \delta_i \lambda)$ does not intersect the inner ball of \overline{S}_i .)

Minimal TT balls and Gabriel simplices. If the center \underline{m}_T of the minimal TT ball \underline{M}_T belongs to the relative interior of a Voronoi face of the tuple, or equivalently the ball is conflict free, the simplex is called *Gabriel*.

Remark. 8. *The minimal TT ball \underline{M}_T is unique, so that a single Voronoi face dual of the tuple T can witness a Gabriel simplex. In particular, for any other Voronoi face of the tuple, the minimal TT ball associated with that face involves at least another toleranced ball. For example, the Voronoi region of \overline{S}_4 in Fig. 11 is split into two Voronoi faces. The center of the minimal TT ball of \overline{S}_4 being located within the Voronoi region of \overline{S}_3 , the dual of each Voronoi face of \overline{S}_4 is not Gabriel. The minimal TT balls of these two faces are in fact associated to the same triple, namely $\overline{S}_2, \overline{S}_3$ and \overline{S}_4 .*

Maximal TT balls and domination of simplices. For a simplex $\Delta(T)$, consider the intersection of the spheres bounding the grown balls, i.e.

$$I_T[\lambda] = \bigcap_{\overline{S}_i \in T} \partial \overline{S}_i[\lambda]. \tag{32}$$

In 3D, if T is a $k + 1$ tuple, $I_T[\lambda]$ is generically a $2 - k$ -sphere. Consider now a tuple such that the δ_i of its balls are not all equal, and assume that $T = A \cup B$, with A the balls realizing the maximum δ_i in the tuple. The corresponding bisector is bounded and has a unique maximal TT ball \overline{M}_T . If this ball is conflict free, the spheres bounding the grown balls in T intersect until $I_T[\lambda]$ reduces to the point \overline{m}_T . Beyond that point, the intersection of the spheres bounding grown balls in B is contained in the union of the grown balls in A . To formalize this behavior, we define—recall that an ancestor of a node in the Hasse diagram is any node found on a path joining this node to that associated with a zero-dimensional simplex:

Definition. 2. *A simplex $\Delta(T)$ whose dual Voronoi face contains the center \overline{m}_T of the maximal TT ball is called dominant.*

A simplex $\Delta(U)$ which is an ancestor of the dominant simplex $\Delta(T)$ in the Hasse diagram, with $B \subset U \subsetneq T$, is called dominated.

As opposed to the Euclidean setting, a dominant simplex $\Delta(T)$ does not catch a coface when point \overline{m}_T is reached by the growing balls. Similarly, a dominated simplex does not catch any coface either when point \overline{m}_T is reached. To identify the moment in time where simplex $\Delta(U)$ gets dominated, we introduce

$$\gamma_{\Delta(U)} = \overline{\rho}_{\Delta(T)}. \tag{33}$$

The condition $B \subset U \subsetneq T$ actually yields 2 cases, namely (i) $U = B$, or (ii) $B \subsetneq U \subsetneq T$. In three dimensions, enumerating these possibilities yields the following cases:

▷ **Dom.1** $T = \{\overline{S}_1, \overline{S}_2\}$ with $\delta_1 > \delta_2$: case (i) that is $U = \{\overline{S}_2\}$.

▷ **Dom.2** $T = \{\overline{S}_1, \overline{S}_2, \overline{S}_3\}$ with $\delta_1 > \delta_2 \geq \delta_3$: case (i) that is $U = \{\overline{S}_2, \overline{S}_3\}$.

▷ **Dom.3** $T = \{\overline{S}_1, \overline{S}_2, \overline{S}_3\}$ with $\delta_1 = \delta_2 > \delta_3$: case (i) that is $U = \{\overline{S}_3\}$, and case (ii) that is $U = \{\overline{S}_1, \overline{S}_3\}$ or $U = \{\overline{S}_2, \overline{S}_3\}$.

By convention and since a 4-tuple yields a discrete set of at most four tetrahedra, we say that a 3-simplex cannot be dominant—which prevents a 2-simplex from being dominated. Also, a 0-simplex cannot be dominant. Dominant and dominated simplices are important to describe the evolution of the boundary $\partial \mathcal{F}_\lambda$: upon getting dominated, a simplex does not contribute to $\partial \mathcal{F}_\lambda$ anymore.

Remark. 9. *A dominant simplex may have cofaces.*

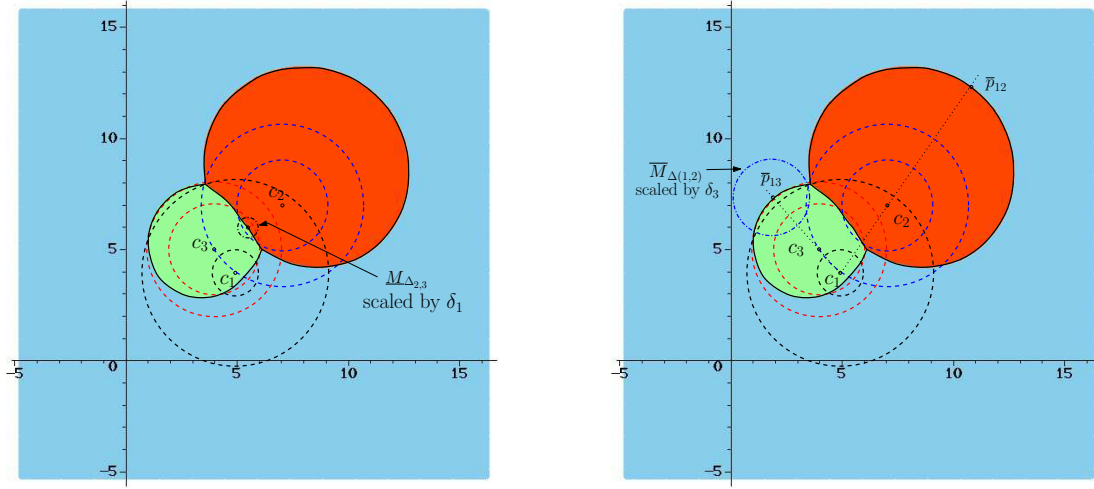


Figure 14: Gabriel, dominant and dominated simplices illustrated with the CW VD of 3 tolerated balls (dashed lines): $\bar{S}_1 = (5, 4; 1, 4)$ (black), $\bar{S}_2 = (7, 7; 2, 3.5)$ (blue), $\bar{S}_3 = (4, 5; 2, 3)$ (red). (Left) The minimal TT ball $\underline{M}_{\Delta(2,3)}$ is conflict free (witnessed by the black dashed-dotted circle): $\Delta(2, 3)$ is Gabriel. Simplices $\Delta(2)$, $\Delta(3)$ and $\Delta(1, 3)$ are Gabriel too. (Right) The max TT ball $\bar{M}_{\Delta(1,3)}$ is conflict free (witnessed by the blue dashed-dotted circle): $\Delta(1, 3)$ is dominant and $\Delta(3)$ is dominated. $\Delta(1, 2)$ is dominant and $\Delta(2)$ is dominated too.

4.2 The λ -complex Filtration

The filtration. Equipped with Gabriel simplices, the following mimics the Euclidean setting:

Definition. 3. The λ -complex K_λ is a subset of the dual complex defined as follows: a simplex $\Delta(T)$ belongs to K_λ iff (i) $\Delta(T)$ is Gabriel and $\lambda \geq \rho_{\Delta(T)}$, or (ii) $\Delta(T)$ is a face of $\Delta(U)$ with $\Delta(U) \in K_\lambda$.

Increasing λ results in a nested sequence of (abstract) simplicial complexes, which eventually coincide with the dual complex, so that the collection of λ -complexes forms a filtration. At the far left of the spectrum, the first non empty simplicial complex (generically) consists of a dual vertex which appears at $\lambda = \Lambda_{\min}$ defined by:

$$\Lambda_{\min} = \min_{\bar{S}_i \in \mathcal{S}} \left(-\frac{r_i^-}{\delta_i} \right). \quad (34)$$

For a large enough λ , the λ -complex matches the dual complex. Since there may be no new Gabriel simplex in the last λ -complex, this holds for $\lambda \geq \Lambda_{\max}$ with

$$\Lambda_{\max} = \max \left\{ \max_{\Delta \text{ Gabriel}} (\rho_\Delta), \max_{\Delta \text{ dominant}} (\bar{\rho}_\Delta) \right\}. \quad (35)$$

Remark. 10. Consider Eq. (35). If the last event in the λ -complex does not correspond to the addition of a Gabriel simplex, it actually corresponds to a status change, namely a dominant simplex becomes Interior. See Table 1.

Status of simplices. The status of a simplex in the affine setting is described from the topology of its link. In the CW case, the presence of simplices without any coface as described in section 3.2 requires devising different classification criteria. For a simplex $\Delta(T)$, consider the intersection $I_T[\lambda]$ of Eq. (32). Upon increasing λ , this intersection sweeps the Voronoi region of the tuple. We base our classification on the portion of the Voronoi region swept by $I_T[\lambda]$ up to time λ . That is, a k -simplex of K_λ is classified as follows:

- *Singular*: the region swept by $I_T[\lambda]$ up to time λ is contained in the relative interior of the dual of the simplex.
- *Interior*: the region swept by $I_T[\lambda]$ up to time λ contains the dual of the simplex in its interior.
- *Regular*: neither singular nor interior.

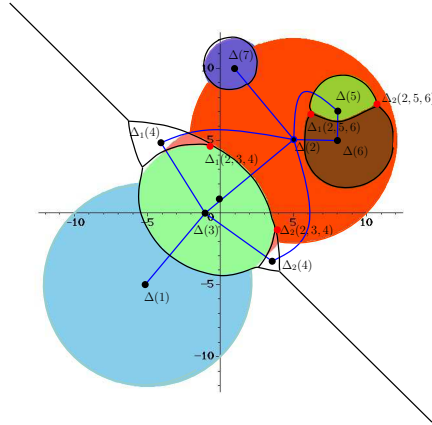


Figure 15: Restricted Voronoi regions for the CW VD of Fig. 11 for $\lambda = 1$, and classification of edges in the λ -complex. Classification of the 8 dual vertices—black dots: $\Delta(5)$ and $\Delta(6)$ are interior and all other dual vertices are regular. Classification of the 10 dual edges—blue edges: $\Delta(1, 3)$ and $\Delta(2, 7)$ are singular; $\Delta(2, 3)$, $\Delta(2, 5)$, $\Delta(2, 6)$, $\Delta(5, 6)$ are interior; the remaining edges are regular. The 4 dual triangles in the λ -complex are represented by red dots vertices.

4.3 Classification of Simplices

Our classification of simplices follows the framework of the affine case [Ede92]. For simplices which are neither dominant nor dominated, in addition to the weight $\rho_{\Delta(T)}$ of the minimal TT ball, we denote $\underline{\mu}_{\Delta(T)}$ and $\bar{\mu}_{\Delta(T)}$ the λ -values such that the simplex becomes regular and interior. For dominant simplices, we also use the weight of the maximal TT ball $\bar{\rho}_{\Delta(T)}$, and the quantity $\gamma_{\Delta(U)}$ introduced in Eq. (33).

For the affine α -complex, the classification of a simplex as singular, regular, or interior requires considering the four cases $\{ \text{Gabriel, not Gabriel} \} \times \{ \text{on the convex hull, not on the convex hull} \}$. For simplices which are neither dominant nor dominated, these four possibilities are also found in the CW case—lines 1-4 of Table 1.

On the other hand, dominant and dominated simplices are not found on the convex hull—each such simplex involves at least one non-maximal ball, and always end up interior since the maximal TT ball of the tuple of a dominant simplex is conflict free. For dominant simplices, the two additional cases to be considered are Gabriel and non Gabriel—lines 5-6 in Table 1. Such a simplex becomes interior as soon as $\lambda \geq \bar{\rho}_{\Delta(T)}$. Similarly for dominated simplices, the two additional cases to be considered are Gabriel and non Gabriel—lines 7-8 in Table 1. Recall that a dominated simplex is always associated to a dominant simplex. Using the weight $\gamma_{\Delta(T)}$ of the maximal TT ball of the tuple of the dominant simplex associated to the dominated simplex, see Eq. (33), the dominated simplex becomes interior as soon as $\lambda \geq \gamma_{\Delta(T)}$.

These notions are illustrated on Fig. 15, which features the restricted Voronoi diagram, i.e. the grown balls restricted to their Voronoi regions. Note in particular that the status of simplices reads from the relative position of the restriction w.r.t. the associated Voronoi face, as specified in section 4.2.

	singular	regular	interior
(1) $\Delta(T) \in CH(\overline{\mathcal{S}})$, Gabriel, non dominated/dominant	$(\underline{\rho}_{\Delta(T)}, \underline{\mu}_{\Delta(T)}]$	$(\underline{\mu}_{\Delta(T)}, +\infty]$	
(2) $\Delta(T) \in CH(\overline{\mathcal{S}})$, non Gabriel, non dominated/dominant		$(\underline{\mu}_{\Delta(T)}, +\infty]$	
(3) $\Delta(T) \notin CH(\overline{\mathcal{S}})$ Gabriel, non dominated/dominant	$(\underline{\rho}_{\Delta(T)}, \underline{\mu}_{\Delta(T)}]$	$(\underline{\mu}_{\Delta(T)}, \overline{\mu}_{\Delta(T)}]$	$(\overline{\mu}_{\Delta(T)}, +\infty]$
(4) $\Delta(T) \notin CH(\overline{\mathcal{S}})$, non Gabriel, non dominated/dominant		$(\underline{\mu}_{\Delta(T)}, \overline{\mu}_{\Delta(T)}]$	$(\overline{\mu}_{\Delta(T)}, +\infty]$
(5) $\Delta(T) \notin CH(\overline{\mathcal{S}})$ Gabriel, dominant	$(\underline{\rho}_{\Delta(T)}, \underline{\mu}_{\Delta(T)}]$	$(\underline{\mu}_{\Delta(T)}, \overline{\rho}_{\Delta(T)}]$	$(\overline{\rho}_{\Delta(T)}, +\infty]$
(6) $\Delta(T) \notin CH(\overline{\mathcal{S}})$, non Gabriel, dominant		$(\underline{\mu}_{\Delta(T)}, \overline{\rho}_{\Delta(T)}]$	$(\overline{\rho}_{\Delta(T)}, +\infty]$
(7) $\Delta(T) \notin CH(\overline{\mathcal{S}})$ Gabriel, dominated	$(\underline{\rho}_{\Delta(T)}, \underline{\mu}_{\Delta(T)}]$	$(\underline{\mu}_{\Delta(T)}, \gamma_{\Delta(T)}]$	$(\gamma_{\Delta(T)}, +\infty]$
(8) $\Delta(T) \notin CH(\overline{\mathcal{S}})$, non Gabriel, dominated		$(\underline{\mu}_{\Delta(T)}, \gamma_{\Delta(T)}]$	$(\gamma_{\Delta(T)}, +\infty]$

Table 1: Classification of simplices in the λ -complex. (Top rows) Common classification with α -complex. (Bottom rows) λ -complex specific cases.

4.4 Tracking Topological Events

Consider the space-filling diagram \mathcal{F}_λ . Selected values of λ featured in Table 1 correspond to topological events underwent by \mathcal{F}_λ —in terms of homology groups. Of particular interest for the application sketched in section 6.2 are those events triggering a decrease of the number of connected components of \mathcal{F}_λ . Such events are associated with selected one-dimensional simplices of the dual complex, and the connected components can be maintained by a Union-Find algorithm upon sorting the λ values featured in Table 1. Following classical terminology, the lifetime of a c.c. is called its *topological persistence* [ELZ02, CSEH05].

5 Algorithms

In this section, we present an output sensitive algorithm to compute the dual complex, together with the accompanying algorithms to compute the λ -complex and a variant which we call the *reduced* λ -complex.

5.1 Using a Sentinel Ball

To ease the implementation, denoting \mathcal{T} the input balls and $\overline{\mathcal{T}}_{\max}$ the maximal balls of \mathcal{T} , we define a new ball \overline{S}_{\max} which is the only maximal ball in $\mathcal{S} = \mathcal{T} \cup \overline{S}_{\max}$, and we compute the CW diagram of \mathcal{S} . Note that the neighbors of \overline{S}_{\max} in the CW diagram of \mathcal{S} are the toleranced balls of \mathcal{T} bounding the CW convex hull of \mathcal{T} . To define \overline{S}_{\max} , we successively set its extremal radii and its center $c_{\overline{S}_{\max}}$.

First, the extremal radii are chosen such that \overline{S}_{\max} is maximal. We arbitrarily set $r_{\overline{S}_{\max}}^- = 0$, and set $r_{\overline{S}_{\max}}^+$ so that \overline{S}_{\max} is maximal, that is:

$$r_{\overline{S}_{\max}}^+ = 1 + \max_{\overline{S}_i \in \overline{\mathcal{T}}_{\max}} (\delta_i). \quad (36)$$

To set the center, we first compute the radius λ' of the largest extremal TT ball to all tuples (pairs, triples, quadruples) of toleranced balls in \mathcal{T} . (Because of domination, we need to process not only quadruples but also pairs and triples.) Consider now a toleranced ball $\overline{S}_i \in \mathcal{T}$. Center $c_{\overline{S}_{\max}}$ is chosen such that the radius of the smallest TT ball of the pair $(\overline{S}_i, \overline{S}_{\max})$ is larger than λ' , $\forall i$. (It is in fact sufficient to process toleranced balls which are maximal in \mathcal{T} .) From Eq. (18) with $\alpha = 1$ and $\beta = 1$, this condition reads as:

$$\|c_i - c_{\overline{S}_{\max}}\| \geq \lambda'(\delta_i + \delta_{\overline{S}_{\max}}) + (r_{\overline{S}_{\max}}^- + r_i^-). \quad (37)$$

Without loss of generality, we choose $c_{\overline{S}_{\max}}$ on the z -axis. Since $\lambda'\delta_i + r_i^- \geq 0$ for any toleranced ball $\overline{S}_i \in \mathcal{T}$, squaring Eq. (37) yields the following equivalent degree two condition:

$$f(z_{max}) = \|c_i - (0, 0, z_{max})\|^2 - (\lambda(\delta_i + \delta_{\overline{S}_{\max}}) + (r_{\overline{S}_{\max}}^- + r_i^-))^2 \geq 0 \quad (38)$$

Function $f(z_{max})$ is always positive, or is so for two intervals $(-\infty, z_i^-)$ and $(z_i^+, +\infty)$ with $z_i^- \leq z_i^+$. It is therefore sufficient to set $z_{max} > z_i^+, \forall i$.

5.2 Hasse Diagrams of Tuples and Simplices

Tuples. A tuple reduces to the list of indices of the toleranced balls it contains, and the inclusion between these indices defines a partial order. We shall use it to store selected tuples called candidate tuples into a Hasse diagram denoted $D_{\mathcal{T}}$, see next section.

Simplices. We represent the dual complex by the Hasse diagram $D_{\mathcal{S}}$ introduced in section 3.2. The level $D_{\mathcal{S}}(k)$ features the simplices of dimension k , and the predecessors and successors of a node in $D_{\mathcal{S}}$ respectively represent the faces and cofaces of the corresponding simplex. A node with no successor is called *terminal*. For two consecutive levels $D_{\mathcal{S}}(k)$ and $D_{\mathcal{S}}(k+1)$, the *slice graph* $D_{\mathcal{S}}^{Sl}(k, k+1)$ defined as follows : the nodes of $D_{\mathcal{S}}^{Sl}(k, k+1)$ are those of $D_{\mathcal{S}}(k)$; two such nodes are incident if they share a coface of $D_{\mathcal{S}}(k+1)$.

Hasse diagram $D_{\mathcal{S}}$ and related operations. We endow $D_{\mathcal{S}}$ with two operations to be used for the construction of the dual complex. Consider a tuple T_k . This tuple is said to *identify* a $(k-1)$ -face if the vertices defining this $(k-1)$ -face correspond to the toleranced balls of the tuple. Finally, consider the graph $D_{\mathcal{S}}^{Sl}(k, k+1)$, together with a k -simplex $\Delta(T_{k+1})$ having a $(k-1)$ -face identified by T_k , that is $T_{k+1} = T_k \cup \{\overline{S}_j\}$ for $\overline{S}_j \in \overline{\mathcal{S}} \setminus T_k$. A *restrained connected component* (restrained c.c.) of $D_{\mathcal{S}}^{Sl}(k, k+1)$ anchored at $\Delta(T_{k+1})$ is a c.c. such that all its nodes are identified by the tuple T_k . Consider now the largest c.c. of $D_{\mathcal{S}}^{Sl}(k, k+1)$ containing the simplex $\Delta(T_{k+1})$. Restricting this c.c. to nodes and edges identified by T_k yields one or more c.c. called *unrestrained c.c.* These notions are illustrated on Fig. 17.

Mapping tuples to simplices. As seen in section 3.2, a tuple T possibly yields several simplices. Denoting m the multiplicity of a tuple T_k , we shall use a map $M_{T\mathcal{S}}$ mapping T to the corresponding simplices $\Delta_j(T)$, $j \in 1, \dots, m$. The correspondence between the levels of $D_{\mathcal{S}}$ and $D_{\mathcal{T}}$ is illustrated on Fig. 16. Abusing terminology, we define:

Definition. 4. A simplex of the dual complex is said to be identified by a tuple T if the tolerated balls found in T form a subset of the vertices of the simplex.

The cofaces of the tuple T are the simplices of the dual complex which are identified by T .

Map M_{TS} is used to retrieve the cofaces of a tuple T as follows: first, the successors of T in the Hasse diagram D_T are collected; second, the simplices associated to each successor are accessed thanks to map M_{TS} .

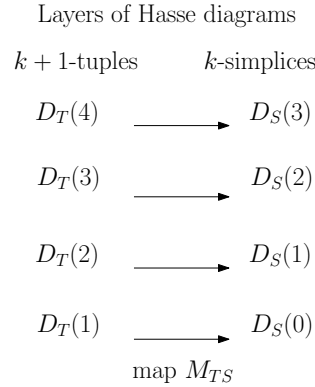


Figure 16: Correspondence between the layers in the Hasse diagram of tuples D_T and the Hasse diagram of simplices of the dual complex D_S .

5.3 Computing Candidate Tuples

A number of practical settings are concerned with growth processes up to a maximum value $\lambda_{\max} < \Lambda_{\max}$ of λ —in the absence of restriction we shall use $\lambda_{\max} = +\infty$. We now define so-called candidate tuples, which will be used in section 5.4.

Definition. 5. A k -tuple with $k \leq 2$ is termed a candidate tuple if its minimal TT ball has a radius less than λ_{\max} . Similarly, a 4-tuple is called candidate if at least one radius of its TT balls is less than λ_{\max} .

We report candidate tuples, from singletons to quadruples. The strategy consists of building the Hasse diagram D_T in a bottom-up fashion, the last two layers being constructed from the layers below. More precisely:

- ▷ A tolerated ball is a candidate singleton provided that $-r_i^-/\delta_i > \lambda_{\max}$. If so, we store in into L_1 .
- ▷ Consider a pair $(\overline{S}_i, \overline{S}_j)$ out of the $\binom{n}{2}$ possibly pairs. The pair is a candidate provided that $\overline{S}_i[\lambda_{\max}] \cap \overline{S}_j[\lambda_{\max}] \neq \emptyset$. If so, we store in into L_2 and set the links to L_1 .
- ▷ For triples and quadruples, we exploit the recursive structure of tuples encoded in the Hasse diagram D_T . Denote L_k the list of candidate k -tuples. We wish to compute L_{k+1} from the lists $L_i, i = 0, \dots, k$ and D_T . Let a be a node from L_{k-1} . For two nodes c and d which are successors of a in the Hasse diagram, one has $|a \cup b| = k + 1$. That is, all candidate $(k + 1)$ -tuples can be formed by examining all pairs of successors of nodes in L_{k-1} . We also set the diagram D_T along the way.

Using this strategy yields the following:

Observation. 1. Denote n the number of tolerated balls and τ' the number of candidates tuples. Computing all candidate tuples has output sensitive complexity $O(n^2 + \tau')$. Moreover, checking that the associated extremal TT balls are conflict free has complexity $O(n(n^2 + \tau'))$.

Proof. The quadratic term comes from the possible $\binom{n}{2}$ pairs. For triples and quadruples, it is sufficient to observe that a k -tuple associated to a $(k - 1)$ -simplex is discovered a number of times equal to the number of its $(k - 3)$ -faces, that is, a triple is discovered three times and a quadruple six times. Whence the output sensitive complexity for triples and quadruples.

For the second part of the claim, observe that for each candidate tuple, one needs to run one (four) iterations on all remaining balls for singletons/pairs/triples (quadruples). \square

5.4 Top-down Construction of the Dual Complex

To build the dual complex, assume that the pre-processing described in section 5.3 has been carried out, with $\lambda_{\max} = +\infty$. The algorithm builds the CW VD from cells to vertices. Three data structures are manipulated. First, the Hasse diagram D_T is used and updated, since some candidate simplices which do not yield simplices are removed. Second, the Hasse diagram D_S is constructed. Finally, the map M_{TS} mapping tuples to simplices is set and used.

5.4.1 Computing $D_S(3)$ or equivalently the 0-skeleton of the CW VD

We examine each candidate 4-tuple, and create one simplex in $D_S(3)$ for each conflict free solution of system (30). Map M_{TS} is set accordingly.

5.4.2 Computing $D_S(2)$ or equivalently the 1-skeleton of the CW VD

Case analysis. This step consists of computing Voronoi edges corresponding to $D_S(2)$ and connecting them to Voronoi vertices associated with $D_S(3)$. We consider the candidate 3-tuples. Each such tuple possibly contributes one or more Voronoi edges, and we face three cases. Assume that the cofaces of the tuple have been collected thanks to map M_{TS} .

- ▷ **Vor-1a** If the tuple does not have any coface in $D_S(3)$ and its maximal TT ball has a conflict, the simplex does not exist in the dual.
- ▷ **Vor-1b** If the tuple does not have any coface in $D_S(3)$ and has a conflict free maximal TT ball, the simplex is dominant and contributes its full bisector as a Voronoi edge.
- ▷ **Vor-1c** If the simplex has cofaces in $D_S(3)$, assuming that \mathcal{S}_{\max} contains a single ball, it contributes Voronoi edges bounded by Voronoi vertices. This number of vertices is even, and the construction of Voronoi edges is a two-stage process. First we sort the vertices along the bisector. To do so, we process separately the vertices found in the two half-spaces delimited by the plane containing the centers of the toleranced balls. Sorting either set of Voronoi vertices along the bisector is tantamount to sorting the weights of the TT balls associated with these Voronoi vertices. Second, we form the curved Voronoi edges. If the smallest TT ball of the tuple is conflict free, there is a Voronoi edge between the two first Voronoi vertices of each half-space, and this edge determines the remaining Voronoi edges in each half-space. Otherwise, there is a Voronoi edge between the first two Voronoi vertices on each side of the plane – if any.

Algorithms. We examine the cases in turn.

- ▷ **Vor-1a** The sterile tuple is removed from D_T .
- ▷ **Vor-1b** The simplex is created, and the data structures D_S and M_{TS} are updated accordingly.
- ▷ **Vor-1c** Sorting Voronoi vertices along a bisector requires two predicates: the **O**rientation predicate to locate the vertices in the two half-spaces; a comparison of roots of degree four polynomials to compare the radii of extremal TT balls.

In terms of data structures, every simplex created triggers an update of D_S and M_{TS} .

5.4.3 Computing $D_S(1)$ or equivalently the 2-skeleton of the CW VD

Case analysis. This step consists of computing Voronoi 2-faces corresponding to $D_S(1)$ and connecting them to Voronoi edges associated with $D_S(2)$. Building a Voronoi 2-face requires identifying all the bounding Voronoi vertices i.e. Voronoi 0-faces, which are glued together by Voronoi 1-faces. As illustrated on Fig. 17, this is a non trivial task since the Voronoi region of a pair might not be connected, and a face might not be simply connected. Let the *support* of a non simply connected face be the simply connected region which contains it. We consider all the candidate pairs, and for each of them analyze the cofaces collected thanks to map M_{TS} . We face three cases.

- ▷ **Vor-2a and Vor-2b** These two cases are similar to those found for triples : a pair which does not have any coface is either dominant or is not present in the dual complex.
- ▷ **Vor-2c** The third case is the complex one. Using the 1-skeleton of the CW-VD, we identify those cycles bounding the supports, and those bounding holes. To do so, we search the restrained and unrestrained c.c. of $D_S^{sl}(2, 3)$. There are three sub-cases:
 - *Vor-2c-1*. The Voronoi region of the 2-tuple is simply connected : there is one restrained and one unrestrained c.c. which are identical.

- *Vor-2c-2*. The Voronoi region is not connected (the topology of the faces are arbitrary): restrained and unrestrained c.c. differ. An unrestrained c.c. consists of the union of one or more restrained c.c.. If there is only one restrained c.c. in an unrestrained c.c., the cycle is one hole. If not, the cycles bound faces. As an example, consider Fig. 17. Each cycle C_1, C_2, C_3 is a restrained c.c.. There are two unrestrained c.c.: one includes cycles C_1 and C_3 which are connected in the 1-skeleton of the CW VD, the other one is C_2 which is not connected to C_1 and C_3 in the 1-skeleton of the CW VD.
- *Vor-2c-3*. The Voronoi region is connected but not simply connected. The two searches yield several c.c. which are the same for the restrained and unrestrained case.

Algorithms. We focus on the complex case.

▷ **Vor-2c** From an algorithmic standpoint, the computation of restrained and unrestrained c.c. is a two-stage process. To describe it, we denote $T = (\overline{S}_i, \overline{S}_j)$ the two tolerated balls processed. First, the (plain) c.c. of graph $D_S^{Sl}(2, 3)$ are computed. Any c.c. containing nodes identified by the pair T is an unrestrained c.c.. For example, on Fig. 17, the process yields two such c.c., namely the c.c. defined by C_2 , and that involving C_1, C_3 and the blue edges.

Second, we run a union-find algorithm on each such c.c.. More precisely, consider the subset $D_S(3 | T)$, that is the nodes of $D_S(3)$ which are identified by the pair T . These nodes correspond to Voronoi vertices involving the two balls. Similarly, consider the subset $D_S(2 | T)$ of nodes of $D_S(2)$ which are identified by the pair T . These nodes of D_S correspond to Voronoi edges involving the two balls. We run a union-find process with node set $D_S(3 | T)$ and edge set $D_S(2 | T)$. As illustrated on Fig. 17, this process yields the restrained c.c..

In terms of data structures, the creation of a simplex triggers an update of D_S and M_{TS} .

Remark. 11. For case *Vor-2c-2*, we do not know which faces of the Voronoi region bound cycles defining holes. However, this information is irrelevant if we only focus on the neighborhood relationship between Voronoi regions.

Remark. 12. For case *Vor-2c-3*, one can further identify the cycle bounding the support. Let \overline{S}_i and \overline{S}_j be the tolerated balls of the pair. Consider a cycle C , and let δ_C be the maximum δ of the tolerated balls involved in Voronoi edges and vertices along C —and different from \overline{S}_i and \overline{S}_j . If $\delta_C < \min\{\delta_i, \delta_j\}$, then cycle C bounds a hole, and reciprocally. To see why, consider the bisector of the tolerated balls associated to δ_C and $\min\{\delta_i, \delta_j\}$: it bounds the Voronoi region of the tolerated ball associated to δ_C iff $\delta_C < \min\{\delta_i, \delta_j\}$.

5.4.4 Computing $D_S(0)$ or equivalently the 3-skeleton of the CW VD

Case analysis. This step consists of computing Voronoi 3-faces corresponding to $D_S(0)$ and connecting them to Voronoi 2-faces associated with $D_S(1)$. Building a Voronoi cell requires identifying all the bounding Voronoi edges i.e. Voronoi 1-faces, which are glued together by Voronoi 2-faces. To do so, the difficulties are identical to those faced to compute the 2-skeleton since the topological complications are the same—non connectedness and non-simply connectedness. Analyzing the cofaces found for each tolerated ball yields the following two cases.

▷ **Vor-3a** If a tolerated ball has no coface, its Voronoi region is empty.

▷ **Vor-3b** If a tolerated ball has at least one coface, we use the algorithm computing $D_S(1)$ using $D_S^{Sl}(1, 2)$ instead of $D_S^{Sl}(2, 3)$. Note that if two dual triangles have a common bounded dual tetrahedron, they share at least one dual edge.

Algorithms. Tuple T consisting of a single ball, to glue Voronoi 1-faces thanks to Voronoi 2-faces, union-find is run on the node set $D_S(2 | T)$ and edge set $D_S(1 | T)$.

5.4.5 Complexity analysis

Denote $\text{Sorting}(A)$ the cost of sorting set A , and $\text{Union-find}(A, B)$ the cost of running a union-find algorithm on node set A using the edge set B .

The following observations, which directly stem from the description of algorithms, show that the algorithm constructing the dual complex has output sensitive complexity:

- Computing the 1-skeleton has complexity $\sum_{T \in G_T(3|T)} \text{Sorting}(D_S(3 | T))$
- Computing the 2-skeleton has complexity $\sum_{T \in G_T(2|T)} \text{Union-find}(D_S(3 | T), D_S(2 | T))$

- Computing the 3-skeleton has complexity $\sum_{T \in G_T(1|T)} \text{Union-find}(D_S(2 | T), D_S(1 | T))$

Analyzing these complexities is directly related to the complexity of the CW diagram, an open problem to the best of our knowledge.

It should be noticed, though, that the cubic pre-processing might be optimal in the worst-case. Indeed, the worst-case complexity of the diagram is clearly at least quadratic. And since a Voronoi region can be disconnected, incremental algorithms aiming at finding conflicts may have to exhaustively probe the whole diagram.

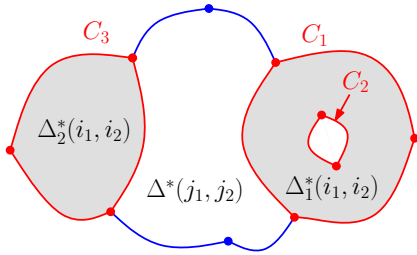


Figure 17: Computing Voronoi faces. Example of two tolerated balls $\overline{S_{i_1}}$ and $\overline{S_{i_2}}$ whose Voronoi region consists of Voronoi faces $\Delta_1(i_1, i_2)^*$ and $\Delta_2(i_1, i_2)^*$ respectively bounded by two and one cycle (C_1, C_2 and C_3) that are restrained connected components (c.c.). Color codes for Voronoi edges and vertices : red: restrained c.c; blue and red: unrestrained c.c.

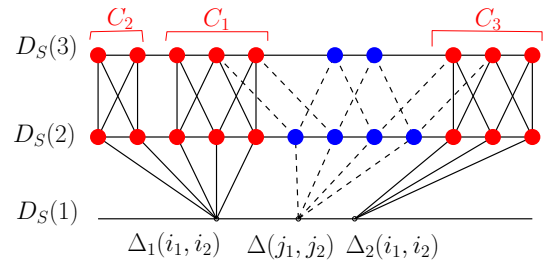


Figure 18: Computing dual simplices. Hasse diagram representation of dual complex of example of Fig. 17. Color of simplices are the same that color of their dual in Fig. 17. Links between simplices whose duals bound the Voronoi faces of the pair $(\overline{S_{i_1}}, \overline{S_{i_2}})$ are represented in solid lines.

5.5 Computing the (reduced) λ -complex

5.5.1 Representation

In the λ -complex, a simplex Δ is attached three tags stating whether (i) it is Gabriel or not, (ii) it contributes to the convex hull $CH(\overline{S})$ or not, and (iii) it is dominant, dominated, or neither one nor the other. Moreover, Δ is endowed with three values delimiting the intervals of a row in Table 1.

5.5.2 Computation

The classical way to compute interval for simplices in the affine α -complex consists of visiting simplices in a top-down fashion, namely from tetrahedra to vertices [Ede92]. In doing so, the status and intervals of a simplex are inferred from those of its cofaces. We apply this strategy for terminal nodes in the Hasse diagram, which are either tetrahedra in $D_S(3)$ or selected dominant nodes of $D_S(2)$ and $D_S(1)$.

5.6 Computation of the reduced λ -complex

Consider the case where one wishes to explore the growth process of the tolerated balls up to a maximum value $\lambda_{\max} < \Lambda_{\max}$ of λ . We call the collection of simplices that appear in the λ -complex for $\lambda \leq \lambda_{\max}$ the *reduced* λ -complex. Computing the reduced λ -complex requires processing a subset of all tuples involved in the entire λ -complex.

Having computed the candidate tuples as indicated in section 5.3, the computation of the reduced λ -complex is identical to that of the entire λ -complex.

6 Implementation and Experiments

6.1 Implementation

Sketch. The implementation follows the CGAL spirit, see <http://www.cgal.org>, and we sketch it in terms of *concepts* (a set of requirements) and *models* (a particular implementation). The class `CW_dual` representing

the dual complex is templated by a combinatorial class providing the Hasse diagram representation, and by a geometric concept class `CWGeometricKernel` providing the predicates and constructions required. The corresponding generic model `CW_geometric_kernel` is itself templated by a concept class `AlgebraicKernel` providing the operations needed to deal with the extremal TT balls. As specified by propositions 2 and 3, computing these TT balls requires solving linear systems or a degree four algebraic equation, while the conflict free test requires evaluating the `conflict_free` predicate of Eq. (10). We implemented a model of the `AlgebraicKernel` named `CW_algebraic_kernel_double` which uses CGAL's `Algebraic_kernel_d_1`—the latter provides efficient operations on univariate polynomials. The number type being `double`, this kernel does not provide exact predicates. Finally, the class `CW_alpha_shape` inherits from `CW_dual` and provides the tags and intervals detailed in Table 1.

Sanity check. To probe the implementation, given a collection of tolerated balls with identical parameters, we checked its ability to compute the Delaunay triangulation of the centers.

Performances. To scale the implementation, we ran it on random collections up to 1000 tolerated balls on a DELL computer with Intel Xeon processor at 3.2 GHz with 2048 Mo of RAM. Balls were generated as follows: the set \mathcal{C} of centers is uniformly generated at random in a cube; for each center c_i , radius r_i^- is set to the length of the shortest edge between c_i and a neighbor of his in the periodic Delaunay triangulation of \mathcal{C} , while r_i^+ is set to the mean between r_i^- and the length of the longest edge between c_i and a neighbor of his in the periodic Delaunay triangulation of \mathcal{C} [CT09].

Statistics for the reduced Dual Complex computation up to $\lambda = 1$ are reported on Fig. 19. We note in particular that the number of candidate tuples increases linearly with the number of tolerated balls, as a linear regression gives a slope of 515 with R-squared value of 0.99. So does the running time, which is about 251 minutes for 1000 tolerated balls.

An example calculation for the whole dual complex of 200 random tolerated balls is illustrated on Fig. 20, with the distribution of λ values associated to Gabriel simplices *and* tetrahedra. (Note that in the affine case, all tetrahedra are Gabriel, a property which does not hold in our case since four balls may contribute four tetrahedra — one of them may be Gabriel.) The whole calculation took about 69 hours for 38,515,103 candidate tuples and 5004 simplices. There are 1971 Gabriel simplices and 1148 tetrahedra. Note that 88,8% of Gabriel simplices and tetrahedra appear in the λ -complex for $\lambda \leq 1$.

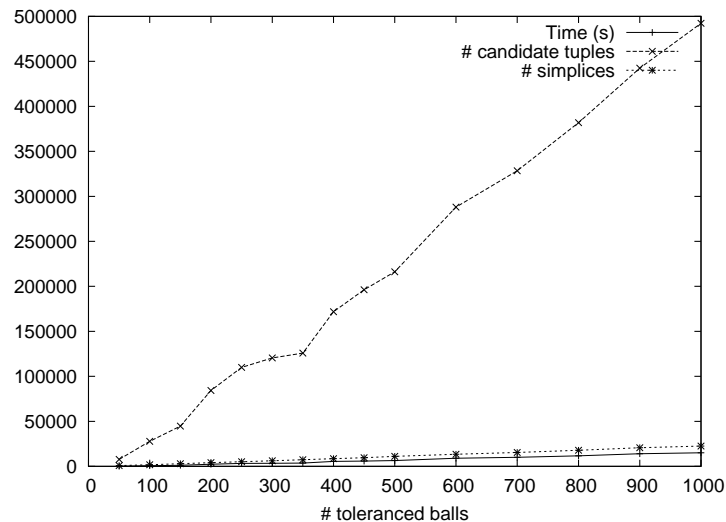


Figure 19: Statistics for the reduced λ -complex up to $\lambda = 1$.

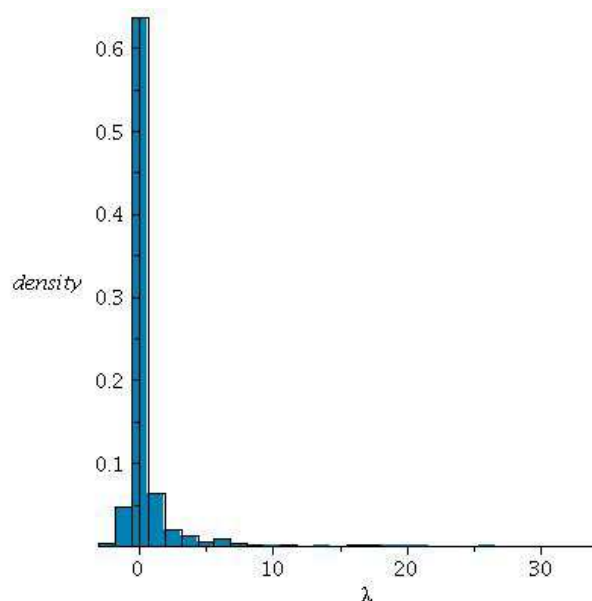


Figure 20: Distribution of λ values associated with Gabriel simplices and tetrahedra for 200 random toleranced balls.

6.2 Application to Molecular Models

Reconstructing Large Assemblies. Understanding the behaviour of living cells requires describing the structure and behaviour of a number of macro-molecular assemblies. While atomic models of small complexes can be obtained from X ray crystallography and/or NMR, the reconstruction of large assemblies such as molecular motors (cell locomotion), branched actin filaments (muscle contraction), chaperonin cavities (protein folding) or nuclear pore complexes (nucleo-cytoplasmic regulation) is more challenging. A recent trend in this context consists of performing the reconstruction from diverse experimental data [AFK⁺08]. For example, cryo electron microscopy (EM) maps allows the reconstruction of envelopes of assemblies, typically at intermediate resolution (10-15 Å). Immuno-labelling combined with EM can be used to locate protein instances, but positioning uncertainties are faced due to the resolution of microscopes. Proteomics methods such as Tandem Affinity Purification provide lists of interacting proteins, but these are inherently ambiguous. The reconstruction of a model from such noisy and ambiguous data is clearly a challenge, and typical reconstruction procedures perform simulating annealing in the space of parameters describing the model, so as to maximize the agreement between this model and the experimental data available. We now examine the largest protein assembly known to date in eukaryotic cells, namely the Nuclear Pore Complex (NPC).

Application to The Nuclear Pore Complex. The NPC is a radially symmetric protein assembly regulating exchanges between the nucleus and the cytoplasm of eukaryotic cells, thanks to the lumen located in its center. The NPC involves 456 protein *instances* of 30 different protein *types*, and we term each connected subset of instances a *complex* in the sequel. The *stoichiometry* of a protein type is the number of its instances—a number in the range 8-16 for the NPC. Two remarkable papers reported putative models of the NPC, reconstructed from the integration of various experimental data [ADV⁺07, AFK⁺08]. A model of the NPC is a collection of balls. The reconstruction resorts to simulated annealing to define the balls (centers and radii) so as to maximize the agreement with experimental data. The whole procedure is very complex—the supplemental of the two Nature papers runs on 107 pages, and different levels of detail are actually used along the optimization procedure. At the finest level, which corresponds to the output, a given protein is represented by a number of balls in the range 1–12, depending on the protein type. The functional optimized being non convex, a total of 1000 models were selected. These models were further averaged to produce one density map per protein type, i.e. a 3D matrix where each pixel is endowed with the probability of being covered by an instance of that type. Refer to Fig. 2 for a 2D example. The maps being quite noisy, contouring a map does not in general allow one to precisely locate the instances of that type. Also, superimposing the 30 maps do not allow one to investigate the relative positions of the instances of all types. We use λ -shapes to make a collective assessment of these maps.

Applications of λ -shapes. As a pre-processing, we build a tolerated model for each map, based on its stoichiometry. The high confidence regions are defined as (clusters of) local maxima of the density. Starting from these anchors, a region growing algorithm is run until a region with prescribed volume is reached. Each connected component is then covered with one tolerated ball. Merging the tolerated models of the 30 types yields a tolerated model of the NPC consisting of 456 tolerated balls. The resulting reduced λ -complex for $\lambda_{\max} = 1$, computed in 11 minutes on an x86.64 bits architecture at 3.2HGz, is used for two purposes.

First, the topological persistence of connected components provides an assessment of the stability of complexes in the assembly. Our particular interest are the *stable* complexes, whose composition in terms of protein types can be discussed w.r.t. the aforementioned Tandem Affinity Purification data. Such a discussion will be reported elsewhere.

Second, we investigate the packing properties of instances : upon increasing λ , the number of connected components ($\#c.c.$) of \mathcal{F}_λ decreases, and its volume Vol_λ increases. The volume of a protein instance being estimated from its sequence of amino-acids, let Vol_{ref} the sum of the volumes of all instances, and denote $r_\lambda = Vol_\lambda / Vol_{ref}$. Tracking the evolution of the number $\#c.c.$ thanks to a Union-Find algorithm applied to the simplices of the dual complex, we investigate the correlations between the three parameters ($\#c.c.$, λ , r_λ). This curve is presented on Fig. 21 for the 32 protein instances of a half-spoke, i.e. one of the 16 sub-units of the NPC. For a perfectly accurate model, one would expect one connected component for a value of $r_\lambda = 1$, but we observe 10 of them in our case. Also, the last two consecutive values of λ triggering a drop of the number of c.c. are as follows: for $\lambda = 0.62$, there are two c.c. and $r_{0.62} = 3.46$; for $\lambda = 1.25$, there is one c.c. and $r_{1.25} = 7.20$. The corresponding grown balls are illustrated on Fig. 22. On this example, the fact that a 7-fold increase of volume occupancy is required to connect the instances hints at an imprecise positioning of selected proteins. In particular, the significant increase of r_λ in-between $\#c.c. = 2$ and $\#c.c. = 1$ hints at a poor positioning of two instances located far away from the 30 remaining ones.

This type of analysis is being used to provide a thorough evaluation of putative pseudo-atomic NPC models, based on (i) the stability of complexes measured by topological persistence, (ii) a coherence analysis of the models w.r.t. Tandem Affinity Purification data, and (iii) quantitative statistics based on volume and surface calculations. These analysis will complement the qualitative discussions and hypothesis developed in [ADV⁺07].

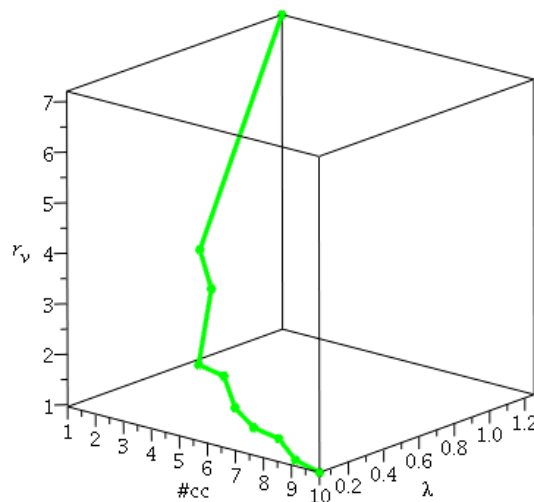


Figure 21: Half-spoke of the NPC : polyline connecting the points ($\#c.c.$, λ , r_λ); the λ values are those triggering a decrease of one unit of the number of connected components.

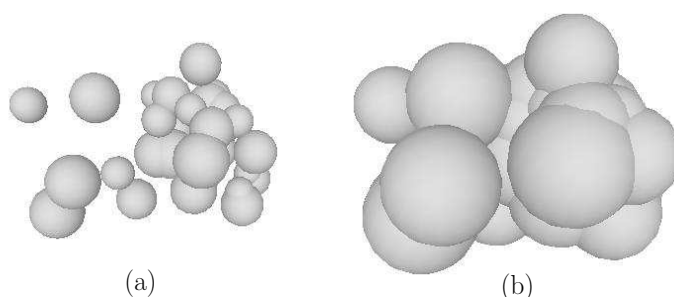


Figure 22: Half-spoke of the NPC : growing the balls so as to end up with a single connected component. The volume of the right domain incurs a 7.2 fold ratio w.r.t. the volume of the isolated protein instances.

7 Conclusion and outlook

Handling ambiguous geometric shapes is non trivial, and the spirit of this work is to integrate modeling uncertainties in the geometric model, as opposed to making arbitrary decisions. As demonstrated, the problem of modeling with toleranced balls is tantamount to using a compoundly weighted Voronoi diagram, and the fact that a toleranced ball (or equivalently a weighted point) has two parameters provides additional modeling flexibility. Yet, a number of further developments are called for.

On the algorithmic side, designing an efficient algorithm to build the dual complex of the CW VD is an open question. While our algorithm fits our needs in molecular modeling, an efficient algorithm is a must for the framework to be used say in geometry processing. From a combinatorial perspective, the task is difficult though, in particular because Voronoi regions are not connected. From a numerical perspective, designing efficient predicates based on degree-four algebraic numbers is also challenging. Finally, the design of toleranced models also raises interesting questions falling in the realm of geometric optimization.

On the application side, toleranced models should have a clear leveraging power in computational structural biology. A major trend there is the reconstruction of large molecular machines from the integration of various experimental data. The models designed so far are not precise enough to be used for mechanistical simulations. We believe that toleranced models have the potential to allow for a precise assessment of such models with respect to biological data, and will help to establish atomic-resolution models.

More classical geometric applications should also benefit from toleranced models, in particular the representation of shapes based on skeletal representations and the medial axis transform, in the spirit of recent contributions such as conformal α -shapes and scale-axis transforms.

Acknowledgements. Svetlana Dokudovskaya is acknowledged for stimulating discussions. Michael Hemmer is acknowledged for his help with CGAL's algebraic kernel.

References

- [ADV⁺07] F. Alber, S. Dokudovskaya, L.M. Veenhoff, W. Zhang, J. Kipper, D. Devos, A. Suprpto, O. Karni-Schmidt, R. Williams, B.T. Chait, et al. The molecular architecture of the nuclear pore complex. *Nature*, 450(7170):695–701, 2007.
- [AE96] N. Akkiraju and H. Edelsbrunner. Triangulating the surface of a molecule. *Discrete Appl. Math.*, 71:5–22, 1996.
- [AFK⁺08] F. Alber, F. Forster, D. Korin, M. Topf, and A. Sali. Integrating diverse data for structure determination of macromolecular assemblies. *Ann. Rev. Biochem.*, 77:11.1–11.35, 2008.
- [BD05] J.-D. Boissonnat and C. Delage. Convex hull and voronoi diagram of additively weighted points. In *ESA*, 2005.
- [BGNC09] B. Bouvier, R. Grunberg, M. Nilges, and F. Cazals. Shelling the voronoi interface of protein-protein complexes reveals patterns of residue conservation, dynamics and composition. *Proteins: structure, function, and bioinformatics*, 76(3):677–692, 2009.

- [BWY06] J.-D. Boissonnat, C. Wormser, and M. Yvinec. Curved voronoi diagrams. In J.-D. Boissonnat and M. Teillaud, editors, *Effective Computational Geometry for curves and surfaces*. Springer-Verlag, Mathematics and Visualization, 2006.
- [CGPZ06] F. Cazals, J. Giesen, M. Pauly, and A. Zomorodian. The conformal alpha shapes filtration. *The Visual Computer*, 22:1–10, 2006.
- [CSEH05] D. Cohen-Steiner, H. Edelsbrunner, and J. Harer. Stability of persistence diagrams. In *ACM Symp. Comp. Geometry*, 2005.
- [CT09] M. Caroli and M. Teillaud. Computing 3D periodic triangulations. *Algorithms-ESA 2009*, pages 59–70, 2009.
- [Ede92] H. Edelsbrunner. Weighted alpha shapes. Technical Report UIUCDCS-R-92-1760, Dept. Comput. Sci., Univ. Illinois, Urbana, IL, 1992.
- [Ede95] H. Edelsbrunner. The union of balls and its dual shape. *Discrete Comput. Geom.*, 13:415–440, 1995.
- [EK06] I.Z. Emiris and M.I. Karavelas. The predicates of the Apollonius diagram: algorithmic analysis and implementation. *Computational Geometry: Theory and Applications*, 33(1-2):18–57, 2006.
- [ELZ02] H. Edelsbrunner, D. Letscher, and A. Zomorodian. Topological persistence and simplification. *Discrete Comput. Geom.*, 28:511–533, 2002.
- [GAG⁺06] Anne-Claude Gavin, Patrick Aloy, Paola Grandi, Roland Krause, Markus Boesche, Martina Marzloch, Christina Rau, Lars Juhl Jensen, Sonja Bastuck, Birgit Dümpelfeld, Angela Edelmann, Marie-Anne Heurtier, Verena Hoffman, Christian Hoefert, Karin Klein, Manuela Hudak, Anne-Marie Michon, Malgorzata Schelder, Markus Schirle, Marita Remor, Tatjana Rudi, Sean Hooper, Andreas Bauer, Tewis Bouwmeester, Georg Casari, Gerard Drewes, Gitte Neubauer, Jens M Rick, Bernhard Kuster, Peer Bork, Robert B Russell, and Giulio Superti-Furga. Proteome survey reveals modularity of the yeast cell machinery. *Nature*, 440(7084):631–636, Mar 2006.
- [GJ03] J. Giesen and M. John. The flow complex: A data structure for geometric modeling. In *ACM SODA*, 2003.
- [GMPW09] J. Giesen, B. Miklós, M. Pauly, and C. Wormser. The scale axis transform. In *ACM Symp. on Computational Geometry*, 2009.
- [LC10] S. Lorient and F. Cazals. Modeling macro-molecular interfaces with interval. *Bioinformatics*, 2010. To appear.
- [LTSW09] K. Lasker, M. Topf, A. Sali, and H.J. Wolfson. Inferential Optimization for Simultaneous Fitting of Multiple Components into a CryoEM Map of Their Assembly. *Journal of Molecular Biology*, 388:180–194, 2009.
- [LWC97] J.-C. Latombe, R. Wilson, and F. Cazals. Assembly sequencing with toleranced parts. *Computer Aided Design*, 29(2):159–174, 1997.
- [Mil63] John W. Milnor. *Morse Theory*. Princeton University Press, Princeton, NJ, 1963.
- [OC00] A. Okabe and B. Boots K. Sugihara S. Nok Chiu. *Spatial Tessellations: Concepts and Applications of Voronoi Diagrams (2nd Ed.)*. Wiley, 2000.
- [SCC⁺06] J. Seo, Y. Cho, C-H. Cho, D. Kim, J. Ryu, and D-S. Kim. The β -shape and β -complex for three-dimensional spheres. *Proceedings of the third International Symposium on Voronoi Diagrams in Science and Engineering*, 2006.

Contents

1	Introduction	3
1.1	Voronoi Diagrams and Applications	3
1.2	Contributions	3
2	Toleranced Models and Compoundly Weighted Voronoi Diagram	4
2.1	Compoundly Weighted Distance and Toleranced Balls	4
2.2	On Concomitant Interpolation Processes	5
2.3	Toleranced Tangency and Generalization of the Empty Ball Property	5
3	The Compoundly Weighted Voronoi Diagram	7
3.1	Bisectors in the CW Case	7
3.1.1	Bisector of two toleranced balls	7
3.1.2	Bisector of three toleranced balls	9
3.1.3	Bisector of four toleranced balls	11
3.2	Voronoi Diagram and its Dual Complex	12
4	Space-filling diagram and λ-complex	14
4.1	Gabriel, Dominant and Dominated simplices	14
4.2	The λ -complex Filtration	16
4.3	Classification of Simplices	17
4.4	Tracking Topological Events	18
5	Algorithms	19
5.1	Using a Sentinel Ball	19
5.2	Hasse Diagrams of Tuples and Simplices	19
5.3	Computing Candidate Tuples	20
5.4	Top-down Construction of the Dual Complex	21
5.4.1	Computing $D_S(3)$ or equivalently the 0-skeleton of the CW VD	21
5.4.2	Computing $D_S(2)$ or equivalently the 1-skeleton of the CW VD	21
5.4.3	Computing $D_S(1)$ or equivalently the 2-skeleton of the CW VD	21
5.4.4	Computing $D_S(0)$ or equivalently the 3-skeleton of the CW VD	22
5.4.5	Complexity analysis	22
5.5	Computing the (reduced) λ -complex	23
5.5.1	Representation	23
5.5.2	Computation	23
5.6	Computation of the reduced λ -complex	23
6	Implementation and Experiments	23
6.1	Implementation	23
6.2	Application to Molecular Models	25
7	Conclusion and outlook	27



Unité de recherche INRIA Sophia Antipolis
2004, route des Lucioles - BP 93 - 06902 Sophia Antipolis Cedex (France)

Unité de recherche INRIA Futurs : Parc Club Orsay Université - ZAC des Vignes
4, rue Jacques Monod - 91893 ORSAY Cedex (France)

Unité de recherche INRIA Lorraine : LORIA, Technopôle de Nancy-Brabois - Campus scientifique
615, rue du Jardin Botanique - BP 101 - 54602 Villers-lès-Nancy Cedex (France)

Unité de recherche INRIA Rennes : IRISA, Campus universitaire de Beaulieu - 35042 Rennes Cedex (France)

Unité de recherche INRIA Rhône-Alpes : 655, avenue de l'Europe - 38334 Montbonnot Saint-Ismier (France)

Unité de recherche INRIA Rocquencourt : Domaine de Voluceau - Rocquencourt - BP 105 - 78153 Le Chesnay Cedex (France)

Éditeur
INRIA - Domaine de Voluceau - Rocquencourt, BP 105 - 78153 Le Chesnay Cedex (France)
<http://www.inria.fr>
ISSN 0249-6399